Article:
Lloyd, GE (2020) Syntectonic quartz vein evolution during progressive deformation. Geological Society, London, Special Publications, 487. pp. 127-151. ISSN: 0305-8719

https://doi.org/10.1144/SP487.3

SYNTECTONIC QUARTZ VEIN EVOLUTION DURING PROGRESSIVE DEFORMATION

Geoffrey E. Lloyd*

School of Earth and Environment, The University, Leeds, LS2 9JT, UK
Orcid: 0000-0002-7859-2486
Corresponding author (e-mail: G.E.Lloyd@leeds.ac.uk)

Running title: *Syntectonic quartz vein deformation*

Abstract: Two models to explain the progressive deformation of syntectonic quartz veins are derived from conventional theories for simple and pure shears. The simple shear model is based on reorientation and changes in length of linear vein elements and predicts initial orientations of veins for imposed shear strains, elongations and strain ratios. The pure shear model considers changes in length of lines variably oriented relative to the maximum compression direction and yields estimates of elongation strains and strain ratios. Expectations of both models are different, as illustrated by analysis of quartz veins from the Rhoscolyn Anticline, Anglesey, NW Wales. The simple shear model recognises three distinct initial orientations, which predict different strains across the fold; the pure shear model suggests veins were initially subparallel to the principal compression direction and predicts effectively constant strains across the fold. In addition, both models predict different patterns of fold vergence: for simple shear, vergence depends on magnitude and direction of shearing and may exhibit complex patterns; for pure shear, vergence patterns are predicted to be essentially constant. In general, the predictions of either model are critically dependent on the origin of the veins, particularly relative to the formation of the Rhoscolyn Anticline.

The publication of '*Folding and Fracturing of Rocks*' (Ramsay 1967) represented a step change in Structural Geology. It cemented the combination of rigorous field investigations augmented by mechanical and numerical analyses in the structural geological psyche and prepared the ground for ever more sophisticated investigations that persist to this day. However, it must be recognised that historically, the book represented a continuous progression of ideas that had developed albeit slowly over more than a century. Although folds and folding are central themes of Ramsay's book (Chapters 7 – 10), fracturing is actually of relatively minor consequence (i.e. there are no chapters dedicated to it specifically); in essence, the presentation is predicated on the significance of stress and particularly strain during geological deformation (Chapters 1 – 6).

This contribution follows the philosophy inherent in '*Folding and Fracturing of Rocks*' to interpret the evolution of syntectonic quartz veins during progressive deformation. The veins occur within (semi-)pelitic units folded by the Rhoscolyn Anticline, Anglesey, NW Wales (Fig. 1), a well-known location for both structural geology research and teaching. It begins with a brief description of the general geology of Rhoscolyn, including the recognition of various models to explain the evolution of the kilometre scale Rhoscolyn Anticline (e.g. Greenly 1919; Shackleton 1954 and 1969; Cosgrove, 1980; Lisle, 1988; Phillips, 1991b; Roper, 1992; Treagus et al., 2003 and 2013; Hassani et al. 2004). However, this contribution is not concerned with (dis-)proving the validity of any of these models; rather, it describes a novel attempt to gain information about the progressive strain history of the Rhoscolyn Anticline by taking numerous geometrical measurements of deformed quartz veins at locations across the fold. As the veins exhibit limited variations in orientation at each locality, it is difficult to perform complete strain analyses at each location without making assumptions about the kinematics of the deformation. Simple shear and pure shear deformations are considered as possible 'end-member' models for the strain history, although other strain histories

are also possible (e.g. combinations of pure and simple shear, etc.). Each model leads to its own set of strain estimates, although the validity of the results hinges on the validity of the assumptions inherent in either model. Thus, this contribution is an example of a relatively new approach to structural analysis based on the *a priori* choice of a number of possible strain history models. A subsequent contribution will consider the models together with other essential details to explain the evolution of the Rhoscolyn Anticline.

Geological setting

Critical awareness of the geology of Anglesey in general and of the Rhoscolyn Anticline in particular (Fig. 1) dates back to the early 19th century (Henslow 1822; see Treagus 2010 and 2017). Successive Geological Survey memoirs (e.g. Ramsay and Salter 1866; Ramsay 1881; and Greenly 1919) provide detailed historical summaries; more recent and relevant contributions are referred to appropriately in the following text.

The Rhoscolyn Anticline and adjacent areas NW and SE (Fig. 1b) occupy a relatively small area of coastal outcrop in the SW of Holy Island, Anglesey, and comprise Monian Supergroup rocks (Fig. 1c). In detail, these consist from oldest to youngest of (e.g. Treagus et al. 2003 and 2013): South Stack Formation (alternating centimetre-metre scale pelites, semi-pelites and psammites), Holyhead Quartzite Formation (typically poorly bedded ortho-quartzites) and Rhoscolyn Formation (alternating centimetre-metre scale pelites, semi-pelites and psammites) of the Holy Island Group and the New Harbour Group (mainly finely laminated green semi-pelites). A (deep-water) turbidite interpretation has been suggested for the original depositional environment of the Rhoscolyn Formation and New Harbour Group, although sedimentary structures indicative of shallower marine environments are present in the South Stack Formation (e.g. Treagus et al. 2013). The abundant chlorite in the pelitic and semi-pelitic units indicates a maximum regional temperature equivalent to lower greenschist facies. As chlorite appears to be present in all deformation-related foliations, this general temperature is considered to have been consistent throughout the deformation history, whether polyphase and/or progressive.

Long thought to be Precambrian in age (e.g. Ramsay 1853; Greenly 1919; Shackleton 1969), recent U-Pb radiometric dating of detrital zircons (Asanuma et al. 2015 and 2017) indicates maximum depositional ages of 569–522 Ma for the lowermost South Stack Formation and 548–515 Ma for the middle New Harbour Group, compatible with a date of 522 ± 6Ma from a detrital zircon in the South Stack Formation (Collins and Buchan, 2004). A subsequent age of ~474 Ma is interpreted as indicating the (Caledonian?) metamorphic event (Asanuma et al. 2017). In addition, recent fossil finds also indicate a lower Cambrian (or younger) age for the Rhoscolyn Formation (e.g. Treagus et al. 2013). Similar trace fossils have been described previously from the Rhoscolyn Formation (Greenly, 1919; McIlroy and Horák 2006) and also rarely from the South Stack Formation (Greenly 1919; Barber and Max 1979). Treagus et al. (2013) have provided evidence of depositional continuity across the boundary between the Rhoscolyn Formation and the base of the New Harbour Group, supporting a common deformational history. Arenig (lower Ordovician) rocks unconformably overlie the Monian Supergroup and provide a minimum age constraint. Overall, the new ages are broadly contemporaneous with the calc-alkaline continental arc magmatism in NW Wales and Central England that formed by successive eastward subduction and closure of the Iapetus Ocean from ca. 711 to 474 Ma (e.g. Asanuma et al. 2017).

The kilometre scale Rhoscolyn Anticline (Fig. 1b) plunges ~22°/063°. The fold shape is asymmetric, with a generally shallowly NW dipping ‘upper’ limb and a steeply SE to locally over-turned and NW dipping ‘lower’ limb, separated by a broad and rounded hinge zone. The inter-bedded quartzites, psammites, semi-pelites and pelites that comprise the Holy Island and New Harbour Groups exhibit strong competence contrasts that permit development of a wide range of mesoscale structures across the fold (e.g. Fig. 2). The presence of these disparate meso-structures

and the relatively small area of generally good outcrop make the Rhoscolyn Anticline a perfect location to teach field structural geology. However, in spite of this attention, debate continues concerning understanding of the evolution of the Rhoscolyn Anticline (e.g. Greenly 1919; Shackleton 1954 and 1969; Cosgrove, 1980; Lisle, 1988; Phillips, 1991b; Roper, 1992; Treagus et al., 2003 and 2013; Hassani et al. 2004)

The pelitic and semi-pelitic units in all formations are characterised by abundant quartz veins, oblique to bedding (e.g. Fig. 2). There is clear field evidence and consensus (Cosgrove 1980; Roper 1992; Treagus et al. 2003; Hassani et al. 2004) that the quartz veins formed parallel to an early cleavage (termed S_1 in Fig. 2). Both the veins and cleavage were subsequently folded (termed F_2 in Fig. 2) consistent with the main Rhoscolyn Anticline and associated minor folds developed on smaller scales on both of its limbs. The behaviour of these quartz veins has been regarded by some (e.g. Cosgrove 1980; Lisle 1988; Phillips 1991b; Roper 1992; Hassani et al. 2004) as being of prime significance for interpreting the origin of the Rhoscolyn Anticline, whilst others (e.g. Treagus et al. 2003) have regarded them as being at best insignificant and at worst misleading. Notwithstanding these alternative views, it is clear that the veins have responded to imposed (progressive) deformation(s) and hence should potentially record evidence of the strain path since their formation.

This contribution focuses on the formation and evolution of the syntectonic quartz veins (Fig. 2). It contests that understanding the development of these veins provides crucial information for any subsequent interpretation of the evolution of the Rhoscolyn Anticline. In the next section, two alternative models are developed, reflecting the contrasting simple and pure shear explanations for the syntectonic behaviour of the quartz veins.

Models for syntectonic quartz vein progressive deformation

It has long been appreciated that syntectonic (quartz) veins afford considerable opportunities for the interpretation of progressive deformation histories (e.g. Ramsay 1967; Fossen 2016). Veins that develop early in (or indeed before) a subsequent (progressive) deformation are modified according to the nature of that deformation. In terms of the Rhoscolyn Anticline, two 'end-member' deformation states appropriate for consideration are simple and pure shear. Two models are developed therefore to consider the potential impact of either of these deformation states on the quartz veins. In both models, the veins are considered to respond passively to flexural slip and as such all folds should be Class 1B, parallel (e.g. Ramsay, 1967). Whilst it is beyond the scope of this contribution to ascertain such behaviour for all veins individually, most do tend to exhibit visually approximately constant thickness and hence can be considered essentially as Class 1B. Furthermore, initial stereographic projection analysis of folded S_0:S_1 lineations about demonstrably F_2 folds of thin, more competent layers within (semi)-pelitic units yields patterns expected for flexural slip folding (Ramsay, 1967, Fig. 8-2). However, the pure shear model proposed by Treagus at al. (2003), amongst others, for the evolution of the Rhoscolyn Anticline, incorporates a buckling mechanism in to the folding process. Consequently, shortening estimates are affected to some degree by vein/host competence contrasts. The adoption of a flexural slip process alleviates the impact of this effect.

Simple shear model

The simple shear model envisages quartz veins developing in an incompetent unit due to progressive shear (e.g. flexural slip) parallel to its boundaries with adjacent competent units (Fig. 3a). The veins are considered to initiate ($\gamma = 0$) as extension fractures, exploiting a mechanical weakness due to an early cleavage (see below), with tips pointing away from the shear sense but are subsequently progressively and passively rotated in the direction of shear. As the initial orientation lies in the shortening field of the imposed (simple) shear deformation, the veins shorten and fold to form sigmoidal tension veins (e.g. Ramsay 1967; Fossen 2016). However, the vein tips are also

translated in the direction of shearing, such that the veins appear to bodily rotate in the shear sense. Consequently, the 'tip-to-tip axis' may eventually rotate through the shear plane normal such that the vein enters the extensional field of the deformation and hence must extend to accommodate further deformation (Fig. 3a); extension may be accommodated by fracture (i.e. boudinage) and/or stretching (i.e. 'unfolding'). Furthermore, as the vein axis rotates through the shear plane normal, the sense of fold vergence changes to opposite that of the shear sense (Fig. 3a).

The behaviour shown in Fig. 3a is readily quantifiable in terms of the initial (α) and final (α') orientations of the vein 'tip-to-tip axis' relative to the shear direction for a simple shear strain (γ) according to (e.g. Ramsay 1967),

$$\gamma = \cot\alpha' - \cot\alpha \qquad (1)$$

This relationship is plotted in Fig. 3b by progressively varying the shear strain for a specific initial angle and calculating the final angle for each combination. The outcome is a series of curves that converge at higher shear strains. However, in practice, for initial angles up to ~150°, it is probably not possible to resolve differences in the final angle for shear strains in excess of ~5.

Use of Fig. 3b in combination with the deformation of syntectonic quartz veins is based on the following methodology (Fig. 3a). Firstly, it is assumed that an initial vein, length L, deforms via simple shear due to flexural slip within the pelitic units. As the vein tips cannot cross the shear plane, the initial angle between the vein and the shear direction is given by,

$$\alpha = \sin^{-1}(T/L) \qquad (2)$$

where T is the orthogonal distance between vein tips (Fig. 3a). As shown, the vein occupies the contractional field of a dextral simple shear; deformation therefore causes it to shorten by folding. If it is assumed that all shortening is accommodated by folding and there is no thickening and/or thinning of the vein,

$$L = \sum_{i=1}^{n} L_i \qquad (3)$$

where L_i is the length of an individual vein fold segment and n is the total number of segments (Fig. 3a). The angle (α') between the vein and the shear direction at any increment of deformation is therefore given by,

$$\alpha' = \sin^{-1}(T/L') \qquad (4)$$

where L' is the linear distance between the tips of the deformed vein (Fig. 3a). As the initial and final angles between the vein and the shear direction are now known, the shear strain (γ) can be determined from Eqn 1.

An example of this methodology is illustrated for the schematic vein modification shown in Fig. 3a. For each increment of known simple shear (γ), the various parameters (i.e. α, α', L, T, L') can all be measured and/or calculated, such that the incremental position can be plotted on Fig. 3b. The initial angle between the vein and the shear direction by convention is taken as the obtuse value (i.e. 180 – α = 163°). The behaviour therefore follows the 163° 'contour', with the angle (α') between the incrementally deformed vein and the shear direction decreasing as shear strain increases to the practical maximum value of $\gamma \approx 5$ (Fig. 3b).

Elongation strain (e) also occurs during simple shear, where the change in length of a line depends on its initial orientation relative to the principal strain axes. Thus, a line may extend, shorten or, for the dextral shear strain shown in Fig. 3a, exhibit progressive incremental shortening followed by

incremental extension; in the latter case, the finite strain may be contractional whilst the last strain increment is extensional. In terms of the behaviour of the quartz veins during flexural slip accommodated by simple shear, the elongation strain produced by the shear strain is simply (Fig. 3a),

$$e = (L' - L)/L \qquad (5)$$

Applying this equation to the shear strain increments illustrated in Fig. 3a, yields the progressive elongations shown. In addition, if L and L' are defined in terms of sequential increments, the incremental elongational strains can also be expressed; both sets of values are plotted against shear strain in Fig. 3c.

Obviously, as with the shear strain estimation (Fig. 3b), the elongation strain behaviour of the quartz veins during simple shear depends on the initial orientation of the vein relative to the shear direction. Figure 4 considers not only the impact of initial vein orientation on finite and incremental elongation strain estimates but also the relationship between these estimates and those for simple shear strain. In practice, whilst both the shear (γ) and elongation (e) strains are generally unknown, all other parameters can be measured either directly in the field and/or from scaled photographs.

Pure shear model

This model is based on the change in orientation of a line due to pure shear (e.g. Ramsay, 1967), as defined by the elongation (e, where negative is contractional). Consider an initial line (e.g. as defined by an undeformed quartz vein) of length L, oriented at an angle α to the pure shear direction (Fig. 5a). Depending on the value of α, the line lies initially within either the shortening or extending field of the pure shear deformation. As the deformation increases, the line therefore either shortens or lengthens (L'), as well as rotates passively (unless it is parallel or normal to the maximum compression direction) to a new orientation (α') according to (e.g. Ramsay 1967),

$$\tan\alpha' = (X/Y)\tan\alpha \qquad (6)$$

where X/Y is the strain ratio. However, eventually all lines migrate in to the extensional field and hence begin to lengthen. The relationship between elongation and initial and incremental/final angles of the line relative to the maximum pure shear compression direction is illustrated in Fig. 5b. Note that the behaviours converge as either the initial or final/incremental angles approach 90° to the compression direction and/or for increasing strain, with some behaviours being eventually undefinable.

As well as elongation, the behaviour of a linear structure, such as a quartz vein, undergoing pure shear deformation can be considered also in terms of the strain ratio, as defined by the strain ellipse (e.g. Ramsay 1967). The strain ratio is defined as the ratio of the maximum (X) and minimum (Y) principal lengths of the ellipse. The relationship between the initial (X/Y) and final/incremental (X'/Y') strain ratios is illustrated in Fig. 5c. As for elongation, many of the behaviours converge as either the initial or incremental/final angles approach 90° to the pure shear compression direction and for increasing strain, with some behaviours being eventually undefinable.

Finally, the relationship between strain ratio and finite/incremental elongation for initial (α) and final (α') angles relative to the maximum compression direction is plotted in Fig. 5d. Note that for most values of α, elongation is extensional; only for $\alpha < \sim 10°$ do contractional strains persist to high strain ratios.

Results

To investigate the impact of the two models described in the previous section, 174 syntectonic quartz veins from both limbs of the Rhoscolyn Anticline have been analysed according their respective methodologies using carefully oriented and scaled digital photographs (e.g. Fig. 2). Ideally, all photographs could be 'normalised' by orienting them looking down the regional fold plunge. However, this is difficult to achieve in practice as the regional fold plunge varies quite significantly with lithology, even between pelitic and semi-pelitic units, and there are also various local factors that impact on minor fold orientation, particularly in the veins. Thus, wherever possible, each photograph was taken looking down the (average) plunge of the folds of the specific vein.

The results of the analyses of the veins are presented in terms of (Figs. 3 - 5): (1) simple shear modification – determination of initial (α, Eqn. 2) and final (α', Eqn. 4) orientations of veins and bedding-parallel shear strain (γ, Eqn. 1); (2) simple shear modification – determination of, and relationship between, elongation strain (e, Eqns. 3, 5) and strain ratio (X/Y) due to shear strain; and (3) pure shear modification – determination of elongation strain (Eqns. 3, 5) and strain ratio (assuming constant area deformation) relative to the direction of pure shear compression.

Simple shear model

The results of the simple shear model analysis of all quartz veins from the Rhoscolyn Anticline in terms of the determination of their initial and final orientations and shear strain are shown in Fig. 6. Whilst there appears to be significant scatter in the results, three distinct trends can be recognised as defined by the curves based on the general model (Fig. 3a and Eqn. 1): I. veins with initial orientations very close (i.e. <10°) to the shear direction; II. veins with initial orientations within 15-35° of the shear direction; and III. veins with initial orientations at 40-60° to the shear direction. Trend I veins exhibit little change in their initial orientation up to $\gamma \approx 3$, after which their orientation begins to change rapidly up to a maximum of $\gamma \approx 6$. Trend II veins exhibit little orientation change up to $\gamma \approx 1$ but then undergo rapid reorientation up to $\gamma \approx 3.5$, after which their orientation becomes almost constant up to a maximum of $\gamma \approx 6$. Trend III veins exhibit immediate and rapid reorientation up to a maximum of $\gamma \approx 1.75$.

The values of the initial and final vein orientations, as well as the shear strain estimates, are indicated by frequency histograms in Fig. 6. In terms of the initial orientations, there is a dominant modal value of ~155° (i.e. ~25° to the shear direction), with mean and standard deviation of 152 ± 14° (i.e. 14 - 42° to the shear direction). Thus, according to the simple shear model (Fig. 3a), most veins had similar initial orientations close to the (assumed local bedding-parallel) shear direction, such that the veins were initially slightly steeper than the (local) bedding. In contrast, the final orientations are much more dispersed, with a mean and standard deviation of 101 ± 43° but no clearly defined modal value (Fig. 6). However, this distribution is misleading as it does not reflect the precise relationship between initial and final orientations due to shear strain. For example, a combination of initially small misorientations relative to the shear direction results also in small final misorientations for a wide range of shear strains for Trend I veins, whilst initial misorentations typical of Trend II veins would produce a wide range of final misorientations for the same range of strains. Similarly, the frequency histogram of shear strains (Fig. 6) represents the same composite of different behaviours. For example, the same shear strain magnitude (e.g. $\gamma \approx 2.5$) can be responsible for very different final orientations (i.e. 40 - 170°) depending on the value of the initial vein orientation (i.e. 120 - 175°), as defined by Trends I – II. The frequency histograms therefore are composites of different behaviours between initial and final orientations and shear strain; this aspect will be considered further in the discussion.

The relationship between shear and elongation strains during simple shear deformation of the quartz veins is illustrated in Fig. 7a. Most veins plot along the $\alpha = 160°$ contour (where α is the initial

angle between the vein and the shear direction), although some also plot along the $\alpha = 165°$, $\alpha = 155°$ and possibly the $\alpha = 130\text{-}135°$ contours. Nevertheless, all trends recognised indicate that quartz veins were initially oriented consistently 10 – 50° steeper than the (local bedding-parallel) shear direction for a simple shear deformation regime. Furthermore, all finite elongation strains remained contractional, although it is not possible to determine the incremental elongational strains.

The simple shear modification of quartz veins can also be interpreted in terms of strain ratio (Fig. 3). Results are shown in Fig. 7b for all veins. In general, strain ratios are lognormally distributed with a clear modal value of ~7.5:1, although many veins indicate strain ratios significantly greater than this modal value.

Pure shear model

The first task in applying the pure shear model (Fig. 5a) is to estimate the relationship between the pure shear compression direction and the initial orientation (α) of the quartz veins. This is achieved by calculating the elongation for each vein using Eqn. 5 and plotting the data on the template provided by Fig. 5b. The results for all veins (Fig. 8a) indicate that they exhibit only contractional finite strains, with a distinct modal value at 10-20°. This situation is possible only for veins that had an initial angle of <30° to the pure shear compression direction. The distribution of elongations is more dispersed, with two minor modes recognised at approximately -0.2 and -0.4 (Fig. 8a). Similarly, the distribution of final orientations (α') is also dispersed. It appears therefore that if the quartz veins were deformed due to a pure shear deformation, then the compression direction was effectively sub-parallel to the vein length; such an orientation is compatible with the initial formation of the quartz veins as extensional fractures but demands also that the early cleavage has similar orientation.

If the initial orientation of the quartz veins was sub-parallel to the pure shear compression direction, then the elongations determined define the principal shortening strain (e_y). The equivalent principal stretching strains (e_x) can be estimated from the method outlined previously assuming constant area pure shear. It is then a simple matter to determine the strain ratio for each quartz vein and hence to plot the relationships between elongations, strain ratios and initial and final orientations of quartz veins (Fig. 8). Because the compression direction is sub-parallel to vein length for most veins (Fig. 8a), in principal all results follow the 0° contour for the initial angle between the vein length and the pure shear compression direction (Fig. 8b). However, as this angle may have varied by up to ±20°, with a probable best estimate of ±10°, there is some dispersion in the results. Thus, whilst a distinct modal strain ratio of ~3:1 is indicated for at least 50% of veins, ratios range up to ~50:1, although most are <10:1 (Fig. 8b, c).

Discussion

The results described in the previous section apply to either the simple or pure shear models for the evolution of syntectonic quartz veins during polyphase and/or progressive deformations. As such, they are not expected to be in agreement but they do represent potential, or perhaps mutually exclusive and/or end-member, solutions. Nevertheless, the results are real potential solutions to the imposed deformation states using actual field-based measurements of syntectonic quartz veins. Thus, either model could be deemed valid depending on constraints imposed by other field relationships; for example, as proposed by either Treagus et al. (2003) or Hassani et al. (2004) for the specific case of the Rhoscolyn Anticline.

Summary of results

The results of the application of simple and pure shear models to the quartz veins at Rhoscolyn are summarised in Table 1. The simple shear model is considered in terms of the three trends

316 recognised in the results (Fig. 6), whilst the pure shear model recognises the predicted spread in the
317 initial orientations relative to the compression direction. This summary of the results can be used to
318 design conceptual behaviours for the final ideal/typical configurations of the Rhoscolyn quartz
319 veins due to either simple or pure shear deformations, as follows (Fig. 9).

320 For simple shear, Table 1 and Fig. 9a recognise the three main trends (I, II, III) predicted on the
321 basis of their interpreted initial orientations (α) relative to the (bedding-parallel) shear direction.
322 The behaviour is depicted via the schematic shapes expected for the deformed quartz veins due to
323 the interpreted shear strains (γ). Also indicated are the estimated elongation strains (e), which are all
324 contractional, and strain ratios (X/Y). The two highest shear strains (i.e. γ = 1.25 and 2.5) are not
325 recognised for Trend III in the vein dataset but are shown for completeness.

326 The schematic summary behaviours depicted in Fig. 9a can be represented on the relevant strain
327 analysis plots derived previously (i.e. Figs 5 and 6) and illustrate an important aspect of vein
328 behaviour under simple shear (Fig. 10). Irrespective of the initial orientation of a vein relative to the
329 shear direction, if the shear strain is sufficiently large, it will rotate through the normal to the shear
330 plane and enter the extensional field of the deformation. Such behaviour impacts on the estimation
331 of elongation, which initially begins to exhibit incremental and eventually finite extensional strains
332 (e.g. Trend III in Figs. 9a and 10c), with concomitant impact on strain ratios. Furthermore,
333 stretching of the veins may remove obvious evidence of initial shortening, making shear strain
334 estimation difficult. In addition, the vergence sense indicated by the vein changes as it rotates
335 through the shear plane normal. Thus, care is required in assessing the simple shear model of
336 syntectonic vein deformation; apparently small strains may be a result of superposition of
337 progressive contractional and extensional (simple shear) strain increments.

338 For pure shear, Table 1 and Fig. 9b recognise that the initial orientation (α) of the quartz veins was
339 sub-parallel (up to ±10°) to the pure shear compression direction As it is generally agreed that the
340 veins formed parallel to the early cleavage, this configuration supports the contention that they
341 likely formed as extension fractures. In Fig. 9b, an absolute maximum range of initial angles (α)
342 relative to the pure shear compression (i.e. the maximum principal stress, σ_1) direction of ±20° is
343 indicated for a 'conjugate' vein system, reflecting the possibility of symmetrical orientations due to
344 cleavage fanning; also shown are the contractional elongations (e) and strain ratios (X/Y).

345 The schematic summary behaviours depicted in Fig. 9b can be represented on the relevant strain
346 analysis plots derived previously (i.e. Fig. 8), as shown in Fig. 11. All elongation strains are
347 contractional (Fig. 11a); they are largest when the compression direction is vein-parallel and
348 decrease significantly for a difference in orientation of only ±20°. The strain ratio modal frequency
349 value of 3:1 (Table 1) is independent of the initial and final orientations of the vein relative to the
350 compression direction (Fig. 11b, c).

351 Whilst the results shown in Fig. 11 are relatively simple, they do raise a specific issue; namely, the
352 impact of cleavage fanning on the appearance of syntectonic veins deformed in pure shear,
353 assuming that the veins form parallel to the cleavage. Based on the pure shear results summarised in
354 Table 1 and Fig. 9b, any cleavage fan is restricted to ±20°; however, this spread can be either
355 divergent or convergent upwards (e.g. Fig. 11d, e). The net effect of fanning cleavage is to change
356 the apparent vergence of deformed syntectonic veins. In the example shown, veins formed parallel
357 to the right-dipping cleavage in an upwardly divergent fan (Fig. 11d) would appear to verge to the
358 left, whilst those formed parallel to the left-dipping cleavage would appear to verge towards the
359 right; the opposite configuration applies for an upwardly convergent cleavage fan (Fig. 11e). Veins
360 formed parallel to the pure shear compression direction maintain neutral vergence throughout. Thus,
361 unless the precise nature of the initial cleavage fan is known, it is difficult to interpret the
362 deformation geometry and evolution. The situation is further compounded if the pure shear

363 compression does not act parallel to the fold axial surface, in which case its attitude relative to any
364 cleavage fan is asymmetric. For example, in Fig. 11c, a compression direction plunging 70° 'down-
365 to-the-right' acts at angles from 0 - 40° to the cleavage planes in both divergent and convergent
366 cleavage fans; the type of fan determining the precise relationship between compression direction
367 and cleavage plane. It should also be mentioned that for pure shear, most veins must eventually
368 enter the extensional field of the pure shear with increasing strain; only veins very close to the pure
369 shear (principal) compression direction remain in the contractional field. Consequently, they
370 progressively exhibit initially incremental and eventually finite extensional strains.

371 *Vein location*

372 So far, this analysis of syntectonic veins from Rhoscolyn has considered them grouped together.
373 However, the veins occur across a kilometre scale asymmetric anticline and in simple terms can be
374 distinguished in terms of location on the shallow dipping NW limb, the rounded hinge region or the
375 steep-to-overturned SE limb (Fig. 1b). Unfortunately, whilst vein-bearing lithologies are well-
376 exposed on both the shallow-NW and steep-SE dipping limbs, they are poorly exposed (at least in
377 terms of accessibility) in the hinge region, which is dominated by the massive Holyhead Quartzite.
378 Nevertheless, distinguishing the veins in terms of location reveals some interesting behaviours in
379 terms of both simple and pure shear models (summarised in Figs. 12 and 13 respectively). In
380 particular, it would appear from both models that the strain on the steep SE-limb is generally lower
381 than on the shallow NW-limb. This is a surprising indication as all other available field evidence
382 suggests the opposite.

383 The simplest explanation for the apparent decrease in strains on the steep SE limb is inherent to
384 both the simple and pure shear models (e.g. Figs. 3a, 5a and 9). Both models predict that the initial
385 orientation of the veins is close to the direction of principal strain: For the simple shear model, this
386 orientation is <35° to the simple shear plane (i.e. Trends I and II in Fig. 12a_; for the pure shear
387 model, it is <±20° to the principal pure shear compression direction (e.g. Fig. 11d, e). As such, the
388 initial deformation increments are contractional, expressed by the folding of the veins; however,
389 with increasing strain, the veins eventually enter the (incremental/finite) extensional field and the
390 veins 'stretch'. The product of shortening and extensional strains therefore results in apparently
391 smaller finite strains, particularly where the stretching does not completely 'unfold' the veins.

392 *Strain variations*

393 The 'strain reduction' effect should be most obvious for elongation strain in both simple and pure
394 shear models due to the progressive change from shortening to extension with increasing
395 compression for most vein orientations. In contrast, bulk shear strains (as represented by vein
396 reorientation) and strain ratios should both increase irrespective of the relative proportions of
397 contraction and extension. However, this is not the case as each measure of strain tends to be
398 statistically lower on the steep SE limb (Figs. 12 and 13). It appears therefore that there is another
399 effect in play.

400 Both the simple and pure shear models assume that their respective strain coordinate reference
401 frames are constant throughout either deformation. For the former this is a dextral (SE-verging)
402 shear parallel to the local lithological layering (e.g. Fig. 9a), whilst for the latter it is a steeply SE-
403 plunging principal compression (e.g. Fig. 9b). However, syntectonic veins occur on both limbs of
404 the asymmetrical (overturned to SE) Rhoscolyn Anticline, which exhibits lithological dependent
405 cleavage fanning. Thus, the local relationships between these kinematic deformation systems and
406 the geology (i.e. lithological layering, cleavage and vein orientations, etc.) are unlikely to remain
407 constant during progressive deformation. The critical aspect therefore is the timing of vein
408 formation relative to the formation of the Rhoscolyn Anticline. Given that there is a general
409 consensus that the veins formed parallel to an early (*sic* S_1) cleavage oriented somewhat steeper

relative to the (local) bedding (e.g. Cosgrove 1980; Lisle 1988; Phillips 1991b; Roper 1992; Treagus et al. 2003; Hassani et al. 2004), the simple and pure shear models effectively consider two different large scale structures.

In the case of the simple shear model, both the early cleavage and syntectonic vein formation pre-date the formation of the Rhoscolyn Anticline; they may in fact form in an earlier deformation event entirely. Consequently, whilst initial dextral inter-layer flexural shear may well have acted consistently towards the SE (Fig. 14a), as the Rhoscolyn Anticline developed it would have potentially reversed to become sinistral and NW-verging (i.e. towards the anticlinal hinge) on the steep limb of the fold (Fig. 14c). Thus, the *apparent* shear strain indicated on the SE limb would have reduced, whilst continuing to increase as normal on the NW limb (Fig. 14b). Figure 14d illustrates these behaviours in terms of the change in initial orientation (i.e. $\alpha = 155°$) of the vein axis relative to the (bedding parallel) shear strain (e.g. Fig. 3b). All veins follow the same path (1 – 4) before the formation of the Rhoscolyn Anticline (i.e. $\alpha' = 102°$, $\gamma = 1.93$). However, as the fold evolves, veins on the now shallow NW limb continue along the same path (4a – 5a) because the vergence sense remains SE (i.e. towards the fold hinge); they therefore exhibit a decrease in angle relative to the dextral shear direction (i.e. $\alpha' = 89°$) and increasing shear strain ($\gamma = 2.16$). In contrast, on the now steep SE limb, the vergence sense is NW (i.e. towards the fold hinge); the angle between the veins and the original dextral shear direction (i.e. $\alpha' = 102°$) is now (4b) the initial angle (i.e. $\alpha = 78°$) relative to the new sinistral shear ($\gamma = 0$) (4b). The new path (4b – 5b) therefore links the new initial angle with the final observed angle (i.e. $\alpha' = 47°$) for an apparent finite shear strain of $\gamma = 0.74$. Nevertheless, it is possible to estimate the true finite shear strain by firstly propagating vertically down (i.e. at constant shear strain, $\gamma = 1.93$) from the position of maximum dextral shear stain on the steep SE limb to the $\alpha = 78°$ contour and then following this contour for the magnitude of the dextral shear strain (i.e. $\gamma = 0.74$). Using this approach, the total shear strain on the steep SE limb is estimated to be $\gamma = 2.67$, significantly greater than that estimated for the shallow NW limb.

In the case of the pure shear model, the early cleavage formed a divergent-upwards fan related to the initial upright configuration of the Rhoscolyn anticline (Treagus et al. 2003); the spread of the fan is typically approximately ±20° relative to the vertical axial surface. This initial configuration was subsequently modified by pure shear compression plunging 70° SE (Treagus et al. 2003). The initial spread of the cleavage fan relative to the pure shear compression direction therefore is up to 40° measured in a clockwise (i.e. towards SE) sense (Fig. 15a). According to Treagus et al. (2003), the pure shear compression effected a strain ratio of ~3:1, causing the originally upright fold to overturn and the original hinge to migrate SE, with concomitant rotation and opening of the cleavage fan (Fig. 15a). If the veins formed as extension fractures due to 'opening' of the cleavage planes, this is only possible for orientations up to a maximum of ~40° relative to the compression direction (Fig. 15b, d); in other words, the maximum initial spread of the divergent upwards cleavage fan (Fig. 15a). Cleavage/veins oriented within 40° of the compression direction are initially folded. As the compression direction is a principal direction of the strain ellipsoid, all folds exhibit neutral vergence. As the angle between the veins and the compression direction increases, the folds exhibit increasing vergence; however, the sense of vergence remains constant, top-down-to-NW (Fig. 15a). In addition, veins oriented >20° to the compression direction rotate into the extensional field of the pure shear deformation before the maximum strain ratio is reached and consequently exhibit stretching and perhaps even boudinage; indeed, veins oriented at the maximum of 40° to compression are stretched almost as soon as they are formed. These behaviours are clearly shown by the various strain plots (Fig. 15b-d, lighter shading). Notwithstanding the results for the cleavage fan, the pure shear model analysis of actual vein orientations suggested that they formed within ±10° of the compression direction. In practice, the configuration of the cleavage fan relative to the compression direction restricts the initial vein orientations to within 10° SE of the

latter (Fig. 15a, darker shading). Consequently, the veins are expected to exhibit only a narrow range of contractional elongation strains of ~0.3 - 0.4 for an increase in final orientation of up to ~28° (Fig. 15b-d, darker shading). Furthermore, not only should they show no evidence of extension, whether incremental or finite, but also the vergence sense indicated by the folds should be 'indistinct', ranging from neutral to marginally either upwards or downwards sinistral.

Wider implications

The approach taken in this contribution has been to consider syntectonic quartz veins developed across the Rhoscolyn Anticline, Anglesey, NW Wales, in terms of two end-member models of simple and pure shear. These models are perceived to bracket the various specific deformation models suggested by previous workers (e.g. Greenly 1919; Shackleton 1954 and 1969; Cosgrove, 1980; Lisle, 1988; Phillips, 1991b; Roper, 1992; Treagus et al., 2003 and 2013; Hassani et al. 2004). Depending on their inherent definitions and assumptions, both end-member models provide realistic but different strain estimates and concomitant explanations for a progressive deformation history syn- and post- vein formation. This approach does not provide therefore an unequivocal explanation for the evolution of the Rhoscolyn Anticline; nor does it support unilaterally any of the individual models proposed to date. What it does provide is a framework for future work on this enigmatic structure based on the results, predictions, consequences and expectations of the two end-member models.

Based on the results reported, the behaviour of syntectonic quartz veins during either simple or pure shear depend on three intrinsic factors (Table 2). Firstly, the age, origin and nature of the early (S_1) cleavage, which impact crucially on the formation and initial orientation of the syntectonic quartz veins, relative to the formation of the Rhoscolyn Anticline. Secondly, the vergence sense of folded syntectonic quartz veins. Thirdly, estimates of shear and elongation strains and strain ratio depending on constraints derived by interpretation of the data in terms of either model (i.e. Trends I, II and II for simple shear and an angular range of $0° \leq a \leq 10°$ between the compression direction and the early cleavage for pure shear).

Table 2 clearly indicates significant differences in the predictions of the simple and pure shear models in terms of the behaviours of the syntectonic quartz veins. Nevertheless, it also indicates that vein behaviour, irrespective of model, is predictable depending on the inherent assumptions involved. Thus, whilst detailed analysis *alone* of the syntectonic quartz veins associated with the evolution of the Rhoscolyn Anticline cannot distinguish a priori between simple and pure shear, or indeed some combination of both (i.e. so-called sub-simple or general shear), it cannot be neglected and must form part of an holistic investigation.

Conclusions

This contribution has considered the behaviour of syntectonic quartz veins during (progressive) simple or pure shear deformations. The data used are from the kilometre scale Rhoscolyn Anticline, Anglesey, N. Wales; a popular area for structural geological training and research. In deriving two distinct models for vein behaviour, one based on simple shear and the other on pure shear, this contribution deliberately avoided assessing the validity of previous explanations for the geological evolution of the Rhoscolyn Anticline. In contrast, it concentrated on assessing the relative merits of simple and pure shear as potential end-member deformations. As such, it represents an example of a relatively new approach to structural analysis based on the *a priori* choice of possible strain history models.

Both models depend fundamentally on the initial orientation of the undeformed quartz veins relative to the principal axes of the appropriate deformation. Whilst there is a general agreement that the veins formed (as extension fractures) parallel to an early cleavage, their precise orientation, or

orientation distribution, at the onset of deformation associated with the formation of the Rhoscolyn Anticline remains debatable. Application of each model leads therefore to its own set of vein geometries and strain estimates, with the validity of the results resting on the validity of the assumptions inherent in either model.

For the simple shear model, it is assumed that bedding/layering was sub-horizontal, whilst the early cleavage and hence quartz veins dipped shallowly towards the SE; simple shear acted parallel to bedding/layering, top towards the SE. The model predicts initially SE verging folds with increasing deformation; however, as the original vein axis rotates through the normal to the shear plane, vergence changes polarity.

For the pure shear model, it is assumed that the bedding/layering defined an upright, symmetrical anticline and the early cleavage defined a divergent-upwards fan with a spread of ±20° about the axial surface; pure shear compression acted at 20° to the axial surface, plunging 70° SE. The model predicts folds with opposite or neutral vergence depending on their location relative to the cleavage fan geometry.

Measurements of 174 veins from both limbs of the Rhoscolyn Anticline were input into the models to determine the initial orientations of the veins relative to the axes of the deformations and hence to estimate the simple shear and elongation strains and strain ratios experienced. As anticipated, the models produced different results. For the simple shear case, strain magnitudes decreased with increasing orientation between the shear direction and the initial orientation of the veins. In detail, three distinct 'trends were recognised with initial angles of 180-170°, 165-145° and 140-120°, for which predicted simple shear strains, elongations and strain ratios varied between 3.0 to 0.5, -0.2 to -0.5 and 8:1 to 2:1 respectively. Furthermore, depending on the precise timing of the formation of the Rhoscolyn Anticline, the shear sense on the evolving steeper SE limb of the fold can reverse to become NW, with concomitant reversal of shearing of the quartz veins and an apparent reduction in strain estimates. For the pure shear case, the initial orientations of the veins was subparallel (up to 10° towards the SE) to the compression direction and resulted in more consistent predictions of elongation (-0.36 to -0.42) and strain ratios (3:1).

Whilst this approach in general, and the predictions of the models in particular, should provide significant constraints on future interpretations of the Rhoscolyn Anticline, it is important to emphasise that neither the veins nor any other individual structural element alone can hope to produce a valid interpretation. It is essential that all relevant structures are considered together. Subsequent contributions therefore will need to consider the models together with other essential (structural) geological elements to explain the evolution of the still 'enigmatic' Rhoscolyn Anticline.

Acknowledgements- It is a pleasure to acknowledge the profound influence John Ramsay in general and his book *Folding and Fracturing of Rocks* in particular have had throughout my career; I can still recall buying my copy in 1976 and reading it from cover to cover. Hopefully, this influence is apparent from this contribution. I would like to thank the Society's referees, Sue Treagus, Richard Lisle and Dave McCarthy, for their comments that have helped to improve the initial version of this contribution. I would also like to thank Jacqui Houghton and Ben Craven for contributing photographs, particularly of the quartz veins. Rob Knipe first introduced me to the delights of Rhoscolyn geology in 1985 when I arrived in Leeds; since then I have revisited the area almost yearly with many Leeds and other colleagues on undergraduate structural field classes; however, particular mention must be made of Rob Butler, Jacqui Houghton, Andrew McCaig, Dan Morgan, Jon Mound, Richard Phillips and not least the late and sorely missed Martin Casey. Finally, I dedicate this paper to my mother, Edith Lloyd, who sadly passed away aged 94 during its final writing; not only had she accompanied me on several field classes to Rhoscolyn as she became increasingly infirm but she was a consistent pillar of support throughout my career and life.

References

Asanuma, H., Fujisaki, W., Sato, T., Sakata, S., Sawaki, Y., Aoki, K., Okada, Y., Maruyama, S.,

553 Hirata, T., Itaya, T. & Windley, B. F. 2017. New isotopic age data constrain the depositional age
554 and accretionary history of the Neoproterozoic-Ordovician Mona Complex (Anglesey-Lleyn,
555 Wales). *Tectonophysics,* 706-707, 164-195.

556 Asanuma, H., Okada, Y., Fujisaki, W., Suzuki, K., Sato, T., Sawaki, Y., Sakata, S., Yamamoto, S.,
557 Hirata, T., Maruyama, S. & Windley, B. F. 2015. Reconstruction of ocean plate stratigraphy in the
558 Gwna Group, NW Wales: Implications for the subduction-accretion pro-cess of a latest Proterozoic
559 trench-forearc. *Tectonophysics,* 662, 195–207.

560 Barber, A. J. & Max, M. D. 1979. A new look at the Mona Complex (Anglesey, North Wales).
561 *Journal of the Geological Society, London,* 136, 407–432.

562 Collins, A. S. & Buchan, C. 2004. Provenance and age constraints of the South Stack Group,
563 Anglesey, UK: U–Pb SIMS detrital zircon data. *Journal of the Geological Society,* 161, 743–746.

564 Cosgrove, J. W. 1980. The tectonic implications of some small-scale structures in the Mona
565 Complex of Holy Island, North Wales. *Journal of Structural Geology,* 2, 383–396.

566 Greenly, E. 1919. *The Geology of Anglesey*. Memoir of the Geological Survey, UK.
567 https://archive.org/stream/geologyofanglese01greeuoft/geologyofanglese01greeuoft_djvu.txt

568 Fossen, H. 2016. *Structural Geology*. Cambridge University Press, 2nd ed.

569 Hassani, H., Covey-Crump, S. J. & Rutter, E. H. 2004. On the structural age of the Rhoscolyn
570 antiform, Anglesey, North Wales. *Geological Journal,* 39, 141–56.

571 Henslow, J. S. 1822. Geological description of Anglesea. *Transactions Cambridge Philosophical*
572 *Society*, 1, 359-454.

573 Lisle, R. J. 1988. Anomalous vergence patterns in the Rhoscolyn Anticline, Anglesey: implications
574 for structural analysis of refold regions. *Geological Journal,* 23, 211–220.

575 McIlroy, D. & Horak, J. 2006. Neoproterozoic: the late Precambrian terranes that formed Eastern
576 Avalonia. *In:* Brenchley, P. J. & Rawson, P. F. (eds) *The Geology of England and Wales*. London:
577 The Geological Society, 9–23.

578 Phillips, E. 1991a. The lithostratigraphy, sedimentology and tectonic setting of the Monian
579 Supergroup, western Anglesey, North Wales. Journal of the Geological Society, London, 148,
580 1079–90.

581 Phillips, E. 1991b. Progressive deformation of the South Stack and Hew Harbour Group, Holy
582 Island, western Anglesey, North Wales. *Journal of the Geological Society, London,* 148, 1091–
583 1100.

584 Ramsay, A. C. 1853. On the physical structure and succession of some of the Lower Palaeozoic
585 rocks of North Wales and part of Shropshire. *Proceedings of the Geological Society* 5, 161-178.

586 Ramsay, A. C. 1881. *The Geology of North Wales*. Memoirs of the geological Survey of Great
587 Britain and of the Museum of Practical Geology. Published by HMSO, London.

588 Ramsay, A. C. & Salter, J. W. 1866. The Geology of North Wales and An Appendix on the Fossils,
589 with plates. *Memoirs of the Geological Survey of Great Britain and of The Museum of Practical*
590 *Geology*. Volume III. Published by Longman, Green, Reader, and Dyer, London.

591 Ramsay, J. G. 1967. *Folding and Fracturing of Rocks*. McGraw-Hill, New York.

592 Roper, H. 1992. Superposed structures in the Mona Complex at Rhoscolyn, Ynys Gybi, North
593 Wales. *Geological Magazine,* 129, 475–490.

594 Shackleton, R. M. 1954. The structure and succession of Anglesey and the Lleyn Peninsula.
595 *Advances in Science,* 2, 106-108.

596 Shackleton, R. M. 1969. The Precambrian of North Wales. *In:* Wood, A. (ed.) *The Pre-Cambrian*
597 *and Lower Palaeozoic Rocks of Wales*. University of Wales Press, Cardiff, 1–22.

598 Treagus, J. E. 2010. Greenly and the geological map of Anglesey. *Geoscientist,* 20, 9-11.

599 Treagus, J. E. 2017. In Anglesey with Henslow. *Geoscientist,* 27, 16-18.

600 Treagus, S. H., Treagus, J. E. & Droop, G. T. R. 2003. Superposed deformations and their hybrid
601 effects: the Rhoscolyn Anticline unravelled. *Journal of the Geological Society, London* 160, 117–
602 36.

603 Treagus, J. E., Treagus, S. H. & Woodcock, N. H. 2013. The significance of the boundary between
604 the Rhoscolyn and New Harbour formations on Holy Island, North Wales, to the deformation
605 history of Anglesey. *Geological Magazine* 150, 519-535.

606 **Figure captions**

607 **Figure 1.** (a) General location of the Rhoscolyn Anticline (RA), Holy Island, Anglesey, NW Wales,
608 UK. (b) 3D photogrammetry 'fold profile plane' image produced from point cloud data based on
609 UK OS aerial photographs of the field area; main stratigraphic units also superposed (SSFm, South
610 Stack Formation; HQFm, Holyhead Quartzite Formation, with marker pelite bands; RFm,
611 Rhoscolyn Formation; RA, Rhoscolyn Anticline axial trace). Inset, field view of area indicated by
612 box (broken lines represent schematic bedding). (c) Definition of stratigraphic relationships as
613 currently recognised (e.g. Treagus et al. 2003 and 2013).

614 **Figure 2**. Examples of quartz veins (Q_v) from the South Stack Formation on the shallow-dipping
615 NW limb of the Rhoscolyn Anticline: S0, bedding (which typically defines the local shear plane);
616 S1, early cleavage, which opens to form the veins; S2, later cleavage axial planar to meso-scale
617 folds (F2) and sub-parallel to the Rhoscolyn Anticline axial surface (except where lithologically
618 refracted); L1, pervasive and penetrative S0-S2 intersection lineation, sub-parallel to F2 fold axes.
619 (a) General view showing relationship to meso-scale features. (b) Detail of relatively low shear
620 strain vein (i.e. tip-to-tip line plunges 'down-to-SE', towards the shear direction) showing correct
621 vergence (i.e. 'up-to-SE'). (c) Detail of relatively high shear strain vein (i.e. tip-to-tip line has
622 rotated through the shear plane normal and now plunges 'down-to-NW', away from the SE shear
623 direction) showing incorrect vergence (i.e. 'down-to-NW').

624 **Figure 3.** Simple shear model for (progressive) deformation of syntectonic quartz veins. (a) Model
625 definition (after Fossen 2016); note change in vergence sense of folds with increasing strain.
626 Included also are values of various measurable parameters for positions 0 – 5. (b) Variation in final
627 angle between vein and shear direction for different initial angles (note obtuse sense) to shear
628 direction (α) and different magnitudes of shear strain (γ), according to Eqn. 1 (Ramsay 1967);
629 behaviour of schematic vein in (a) plotted for illustration. (c) Plot of finite and incremental
630 elongation strains for vein in (a) calculated via Eqn. 6.

Figure 4. Impact of initial vein orientation relative to direction of simple shear (obtuse sense), plotted in terms of relationship between shear and elongation strain estimates for simple shear model of vein deformation (Fig. 3a).

Figure 5. Pure shear model for (progressive) deformation of syntectonic quartz veins. (a) General model with values of finite (e) and incremental (e') elongations for pure shear modification of initial linear quartz vein inclined 25° to vertical maximum pure shear compression direction; also indicated are original (X/Y) and deformed (X'/Y') strain ratios. (b) Relationship between finite and incremental elongation strains and initial (α) and final (α') angles relative to maximum compression direction. (c) Relationship between strain ratios and initial and final angles relative to maximum compression direction. (d) Relationship between strain ratios and finite and incremental elongation strains for initial and final angles relative to maximum compression direction. Note, maximum values (5) not plotted in (c) and (d).

Figure 6. Summary of simple shear modification of all measured veins. (a) Shear strain vs. (obtuse) angle to shear direction; note three potential 'trends' (I – III) indicated by shading. (b) and (c) Histograms of initial and final vein orientations respectively relative to shear direction. (d) Histogram of shear strain magnitudes.

Figure 7. (a) Summary of relationship between simple shear strain (γ) and elongation strain (e) for all quartz veins (see Fig. 3c and Eqn. 1); note, practically all data lie in the finite contractional field of the elongation strain. (b) Simple shear induced strain ratios estimated from Eqn. 6 (see Fig. 3c) for all veins.

Figure 8. Summary of pure shear modification of all measured veins. (a) Estimation of initial angle between pure shear compression direction and veins via Eqn. 5 and Fig. 5b (open and closed symbols indicate initial and final orientations respectively); histograms indicate predicted initial (shaded) and final (clear) orientations and (mostly contractional) elongation strain distributions. (b) Relationship between elongation (e), strain ratio (X/Y) and initial (α) and final (α') angles between pure shear compression direction and vein orientation; histograms indicated orientation (horizontal) and (contractional) strain (vertical) distributions. (c) Relationships between estimated strain ratios and initial/final vein orientations relative to pure shear compression direction; histograms indicated strain ratios (horizontal) and initial/final orientation (vertical) distributions.

Figure 9. Summary of results of (a) simple and (b) pure shear models for syntectonic quartz veins; see also Table 1. In (a) three main 'trends' (I – III) recognised on their initial (obtuse) orientations (α) relative to (bedding-parallel, S_0) shear direction are depicted via schematic shapes expected for deformed quartz veins due to interpreted simple shear strains (γ); also represented are elongation strains (e), which are all contractional, and strain ratios (X/Y); note that the two highest shear strains are not recognised for Trend III but are shown for completeness. In (b), maximum range of initial angles ($\alpha < \pm 20°$) relative to pure shear compression direction (σ_1) are depicted for conjugate vein systems, which reflects the possibility of symmetrical orientations due to cleavage fanning, with the most likely state being $\alpha = \pm 10°$; also shown are contractional elongation strains (e) and constant strain ratio (X/Y).

Figure 10. Schematic simple shear model behaviours depicted in Fig. 9a represented on relevant strain analysis plots (open symbols indicate theoretical values). (a) Shear strain for predicted initial (α) and observed final (α') orientations. (b) Strain ratios derived from shear strain estimates. (c) Shear strain vs. elongation; note all elongations are contractional, which restricts initial orientations to >130°.

Figure 11. Schematic pure shear model behaviours depicted in Fig. 9b represented on relevant

strain analysis plots. (a) Predicted initial (α) and observed final (α') orientations (note, broken line represents expected behaviour). (b) Strain ratios vs. (contractional) elongation strains. (c) Relationship between initial/deformed strain ratios and initial/final angle of veins to pure shear compression direction. (d) and (e) Pure shear model applied to veins forming parallel to cleavage in divergent upward and convergent upward cleavage fans respectively.

Figure 12. Impact of vein location (shallow NW limb, hinge and steep SE limb) on simple shear model. (a) Simple shear modification; note Trends I - III indicated by shading. Histograms indicate initial (vertical, shaded) and final (vertical, clear) vein orientations as well as shear strains (horizontal). (b) Relationship between simple shear strain (γ) and elongation strain (e); note, all data lie in finite contractional field of elongation strain. (c) Frequency histograms summarising simple shear induced strain ratios.

Figure 13. Impact of vein location (shallow NW limb, hinge and steep SE limb) on pure shear model. (a) Estimation of initial angle between pure shear compression direction and veins via Eqn. 5 and Fig. 5b; horizontal and vertical histograms summarise elongational strains and initial/final pure shear direction frequencies respectively. (b) Relationship between elongation strain (e), strain ratio (X/Y) and initial (α) and final (α') angles between pure shear compression direction and vein orientation; horizontal and vertical histograms summarise strain ratio and elongational strain frequencies respectively. (c) Relationships between potential strain ratios (frequency histograms) and initial/final vein orientations relative to pure shear compression direction.

Figure 14. Explanation for apparent decrease in strain on steep SE limb of Rhoscolyn Anticline via the simple shear model. (a) Initial (i.e. pre-Rhoscolyn Anticline formation) SE directed shear opens the early 'SE-dipping' cleavage, forming syntectonic quartz veins, which are subsequently folded by bedding parallel shear *in the same sense* across the entire section. (b) and (c) Final (i.e. syn-Rhoscolyn Anticline formation) shear acts in opposite directions on the fold limbs, towards the fold hinge, increasing the shear strain on the NW limb but apparently decreasing it on the SE limb. (d) Estimation of shear strains on the two limbs of the Rhoscolyn Anticline, indicating that contrary to initial observations, the steep SE limb has in fact suffered the higher strain; numbers refer to stages shown in (a) – (c). See text for full explanation.

Figure 15. Explanation for apparent decrease in strain on steep SE limb of Rhoscolyn Anticline via the pure shear model; lighter and darker shading indicate the orientation ranges relative to the pure shear compression direction of the whole divergent upwards cleavage fan (0 - 40°) and the specific results of the field data (0 - 10°) respectively. (a) Initial (top) and final (bottom) configurations of divergent upwards cleavage fan relative to the pure shear compression direction (here plotted vertical for simplicity); also shown are the initial and final strain ellipses and orientations of lines representing the cleavage fan. The initial orientation of the cleavage relative to the pure shear determines whether the veins are folded, stretched or folded and then stretched. (b) - (d) Strain analyses comparing elongation strain, strain ratio and initial and final vein axis orientations relative to the pure shear compression direction.

715 **Table 1.** Summary of the results of the application of simple and pure shear models to quartz vein
716 data from the Rhoscolyn Anticline (N/A, not applicable).

Feature		Simple Shear Model	Pure Shear Model
Initial vein orientation (α)	relative to bedding parallel shear direction	mode: 25° (155°) trend 1: <10° (>170°) trend 2: 15-35° (165-145°) trend 3: 40-60° (140-120°)	N/A
	relative to compression direction	N/A	±10° (compatible with extension fracture origin)
Final vein orientation (α')	relative to bedding parallel shear direction	dispersed – approaching uniform/random (except at lowest angles: >160/20°); significant reorientation for largest strains	N/A
	relative to compression direction	N/A	~35°
Strain estimates	shear (γ)	trend 1: modes at 1.25 & 2.5 trend 2: modes at 1.25 & 2.5 trend 3: 0.75	N/A
	elongation (e)	mode -0.4 (lower on steep SE limb)	mode -0.4 (lower on steep SE limb)
	ratio (X/Y)	mode 7.5:1	typically <10:1; orientation frequency histogram mode at ~3:1

717 **Table 2**. Summary guidelines of strain estimates for the shallow NW and steep SE limbs of the
718 Rhoscolyn Anticline according to the simple and pure shear models.

MODEL	EARLY CLEAVAGE & VEIN AGE	VEIN FOLD VERGENCE		MEAN STRAIN ESTIMATES			
		NW limb	SE limb	Trend	γ	e	SR
SIMPLE SHEAR	Pre-Rhoscolyn Anticline	SE (towards antiform hinge)	SE (away from antiform hinge)	I	≤3.0	≤-0.22	≤8:1
				II	≤1.5	≤-0.50	≤4:1
				III	≤0.5	≤-0.20	≤2:1
		NW (away from anticline hinge)	NW (towards anticline hinge)	I	≥3.0	≥-0.22	≥8:1
				II	≥1.5	≥-0.50	≥4:1
				III	≥0.5	≥-0.20	≥2:1
PURE SHEAR	Syn- (upright) Rhoscolyn Anticline	Neutral to slightly sinistral upwards/downwards depending on initial cleavage fan angle (0°≤α≤10°)		α = 0°	-	-0.42	3:1
				α = 10°	-	-0.36	3:1

719

720

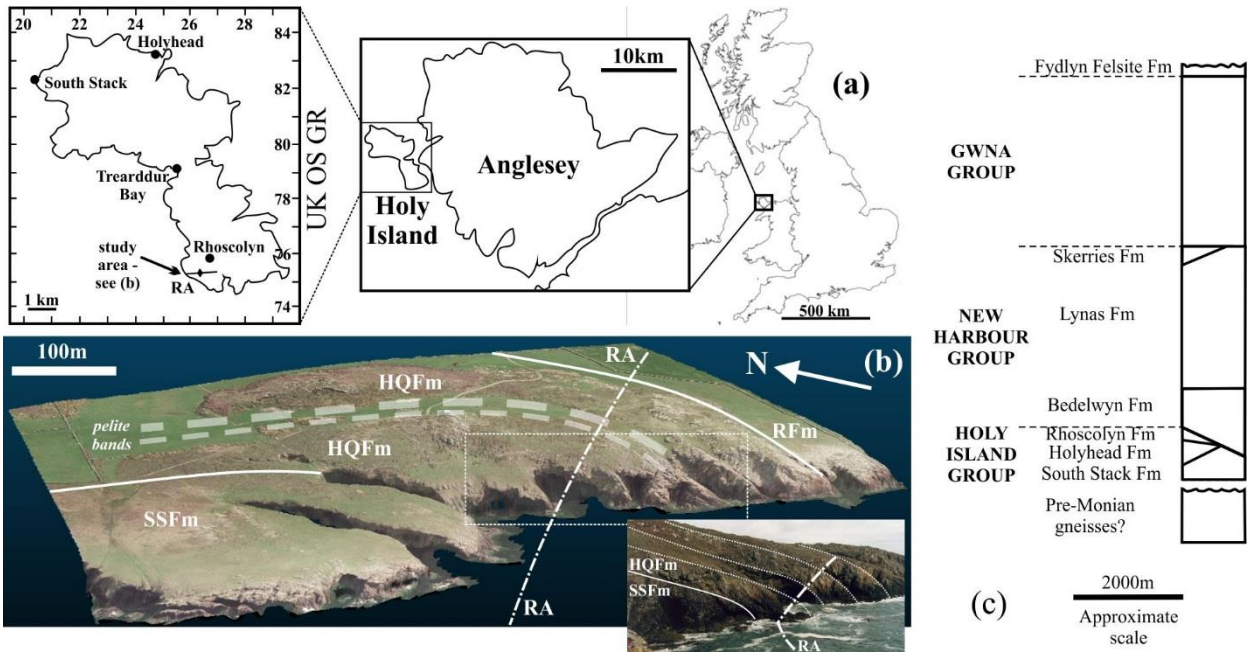

721

722 Figure 1.

723

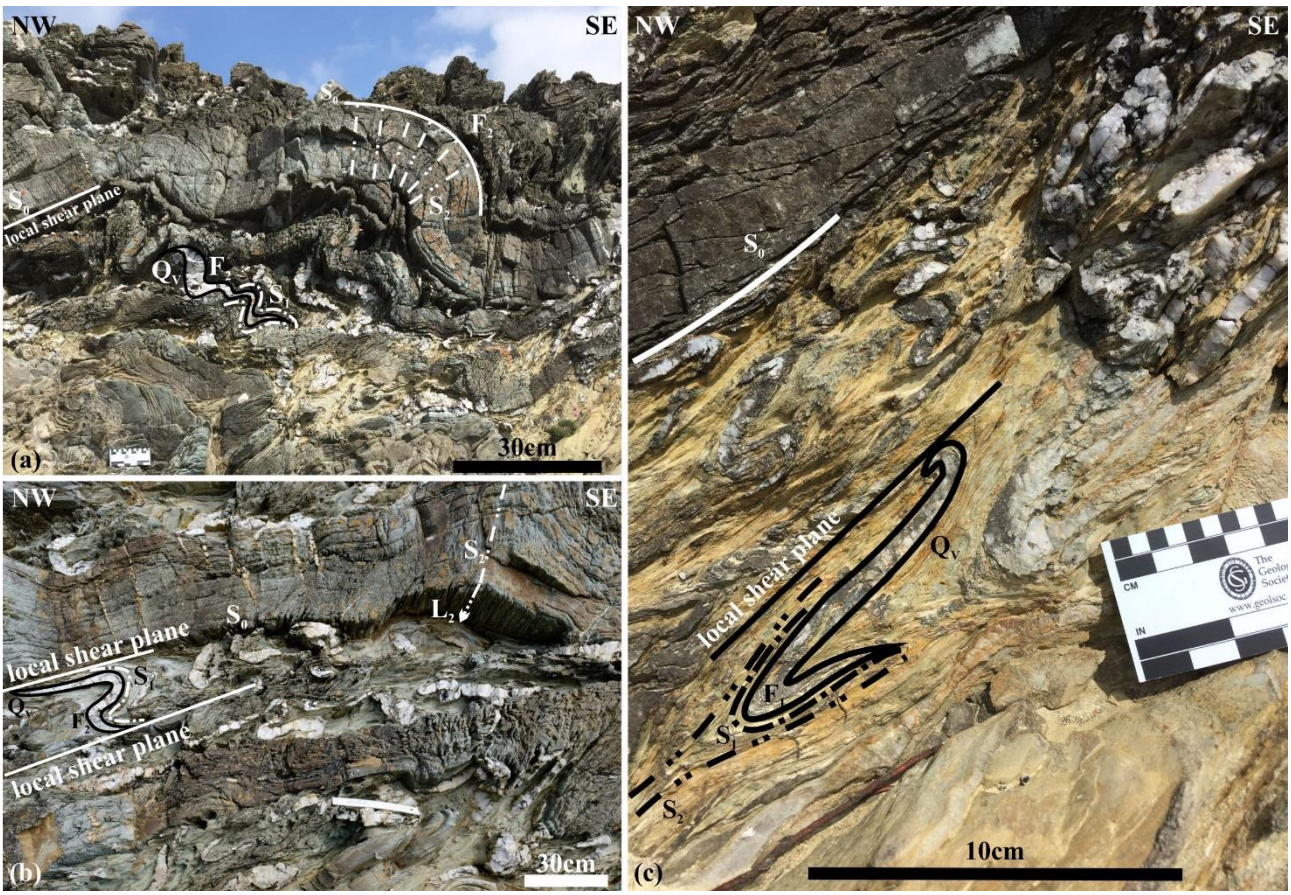
NW
SE
S_0
F_2
S_2
S_0
local shear plane
Q_v
F_1
S_1
30cm
(a)
NW
SE
S_2
L_2
S_0
local shear plane
S_1
Q_v
F_2
local shear plane
30cm
(b)
NW
SE
S_0
local shear plane
Q_v
F_1
S_1
S_2
10cm
(c)

Figure 2.

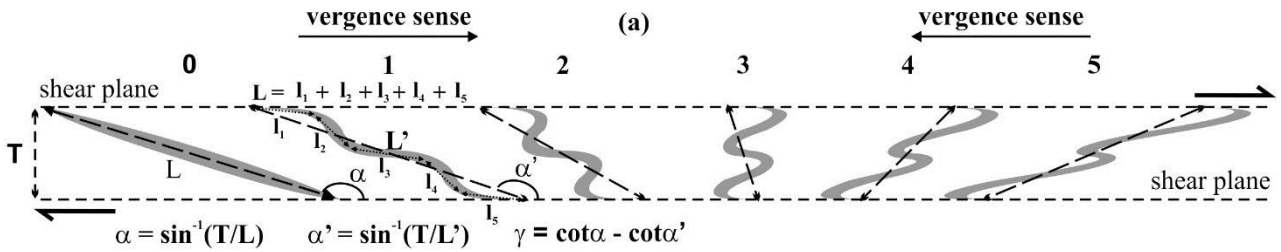

vein angle	α = 163/17°	α' = 161/19°	149/31°	110/70°	51/129°	23/157°
shear strain	γ = 0	0.37	1.61	2.91	4.08	5.63
finite elongation	e = 0	-0.114	-0.421	-0.700	-0.597	-0.256
incremental elongation	e' = 0	-0.114	-0.385	-0.482	0.342	0.849
equivalent strain ellipse						

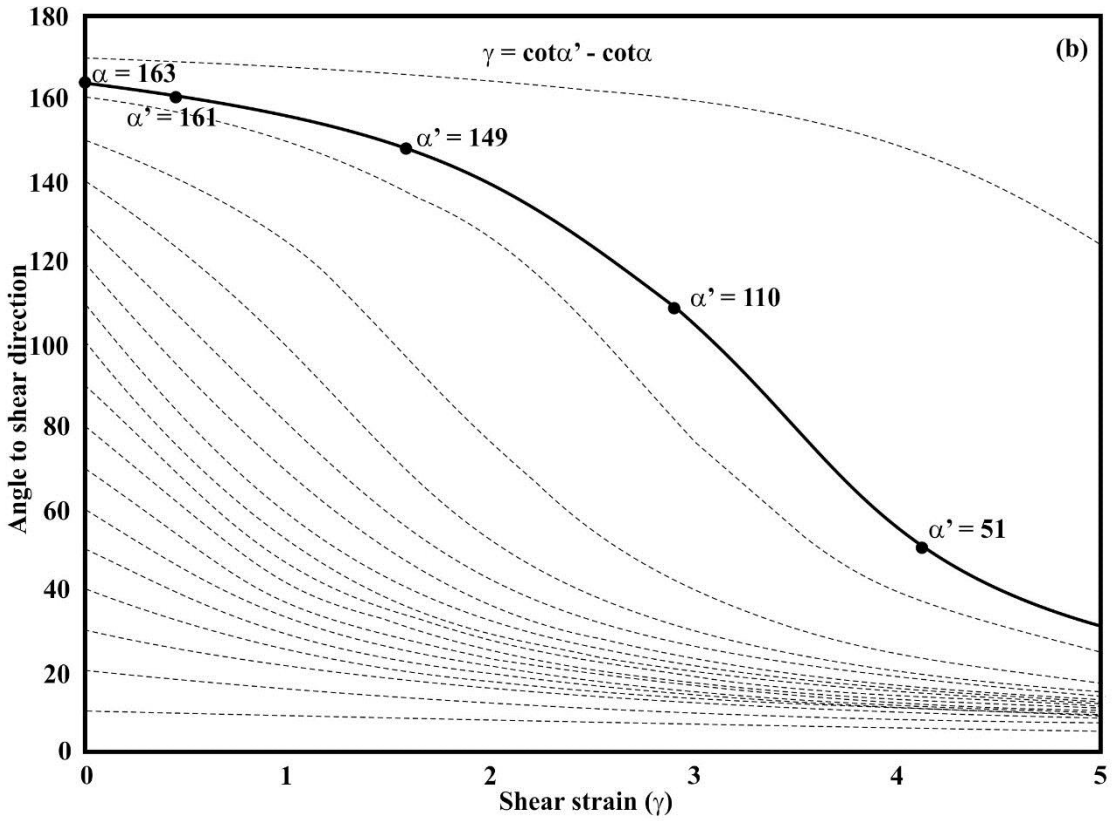

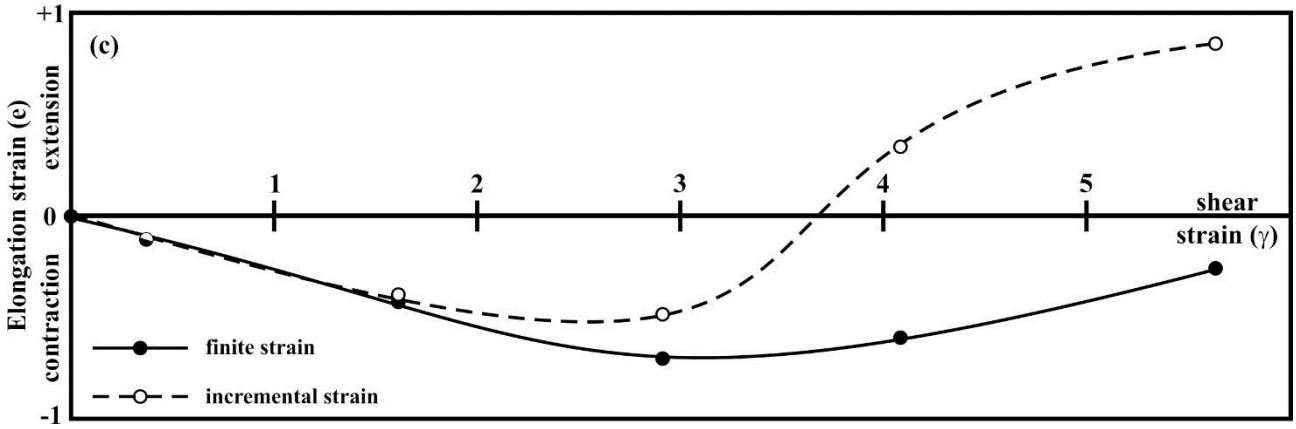

Figure 3

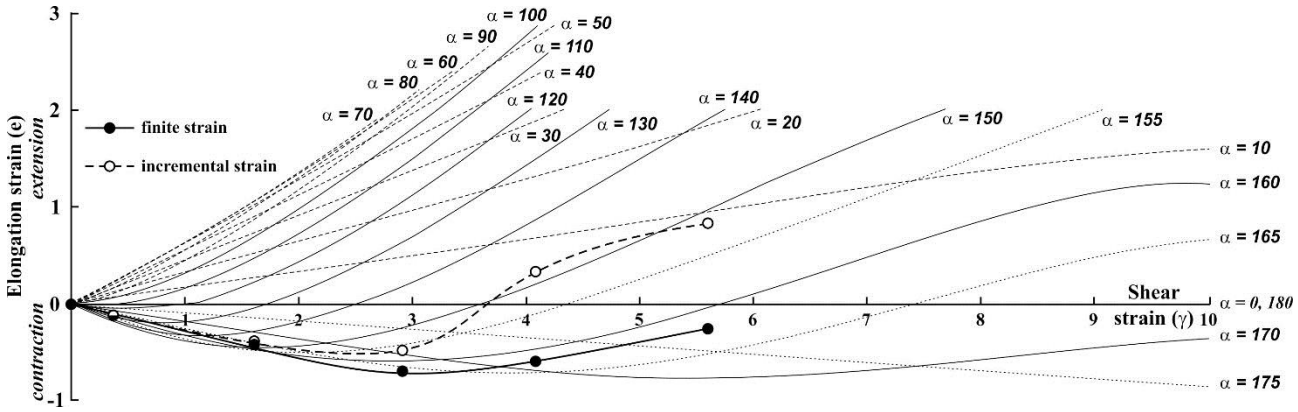
Elongation strain (e)
extension
contraction
finite strain
incremental strain
Shear strain (γ)
α = 100
α = 50
α = 90
α = 110
α = 60
α = 40
α = 80
α = 120
α = 70
α = 30
α = 130
α = 140
α = 20
α = 150
α = 155
α = 10
α = 160
α = 165
α = 0, 180
α = 170
α = 175

Figure 4

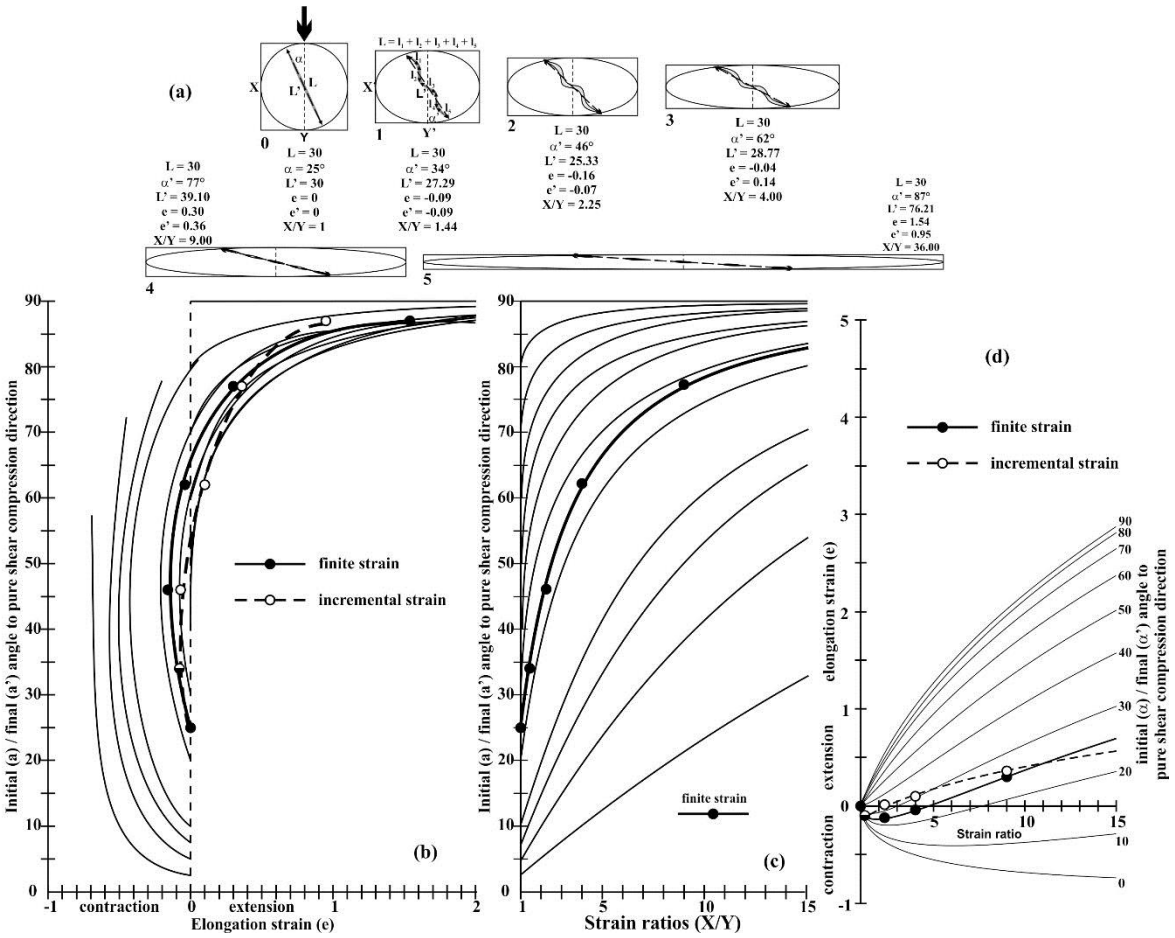
(a)
0
L = 30
α = 25°
L' = 30
e = 0
e' = 0
X/Y = 1
1
L = 30
α' = 34°
L' = 27.29
e = -0.09
e' = -0.09
X/Y = 1.44
2
L = 30
α' = 46°
L' = 25.33
e = -0.16
e' = -0.07
X/Y = 2.25
3
L = 30
α' = 62°
L' = 28.77
e = -0.04
e' = 0.14
X/Y = 4.00
4
L = 30
α' = 77°
L' = 39.10
e = 0.30
e' = 0.36
X/Y = 9.00
5
L = 30
α' = 87°
L' = 76.21
e = 1.54
e' = 0.95
X/Y = 36.00
Initial (a) / final (a') angle to pure shear compression direction
finite strain
incremental strain
contraction
extension
Elongation strain (e)
(b)
Strain ratios (X/Y)
(c)
(d)
elongation strain (e)
extension
contraction
Strain ratio
initial (α) / final (α') angle to pure shear compression direction

Figure 5

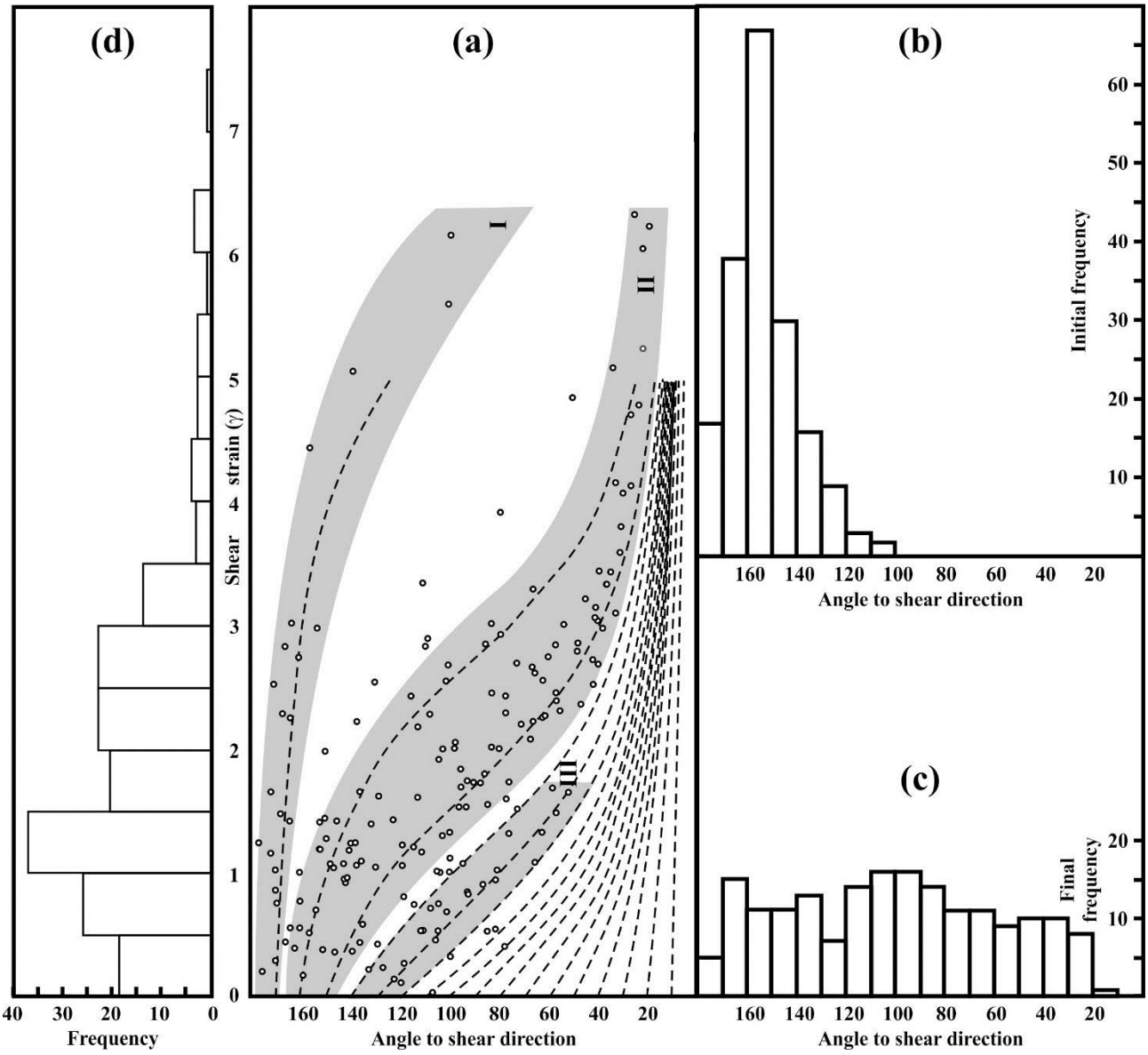
(d)
(a)
(b)
(c)
Shear strain (γ)
Frequency
Angle to shear direction
Initial frequency
Final frequency
I
II
III

Figure 6

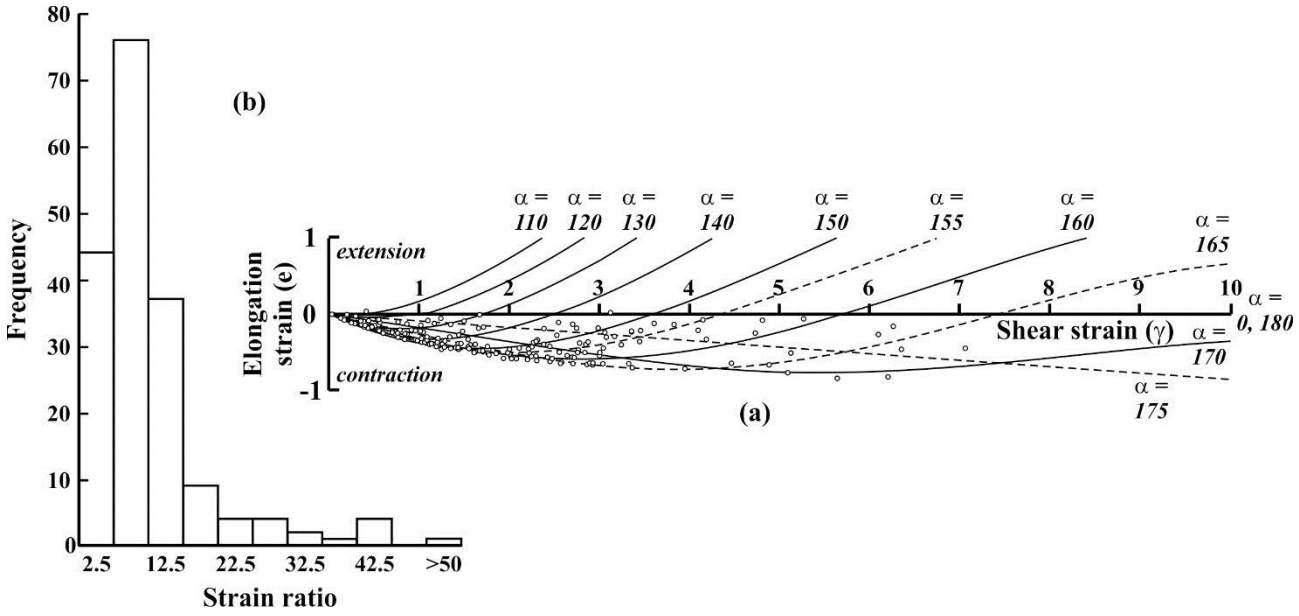
(b)
Frequency
80
70
60
50
40
30
20
10
0
2.5
12.5
22.5
32.5
42.5
>50
Strain ratio
α = 110
α = 120
α = 130
α = 140
α = 150
α = 155
α = 160
α = 165
α = 0, 180
α = 170
α = 175
Elongation strain (e)
1
0
-1
extension
contraction
1
2
3
4
5
6
7
8
9
10
Shear strain (γ)
(a)

Figure 7

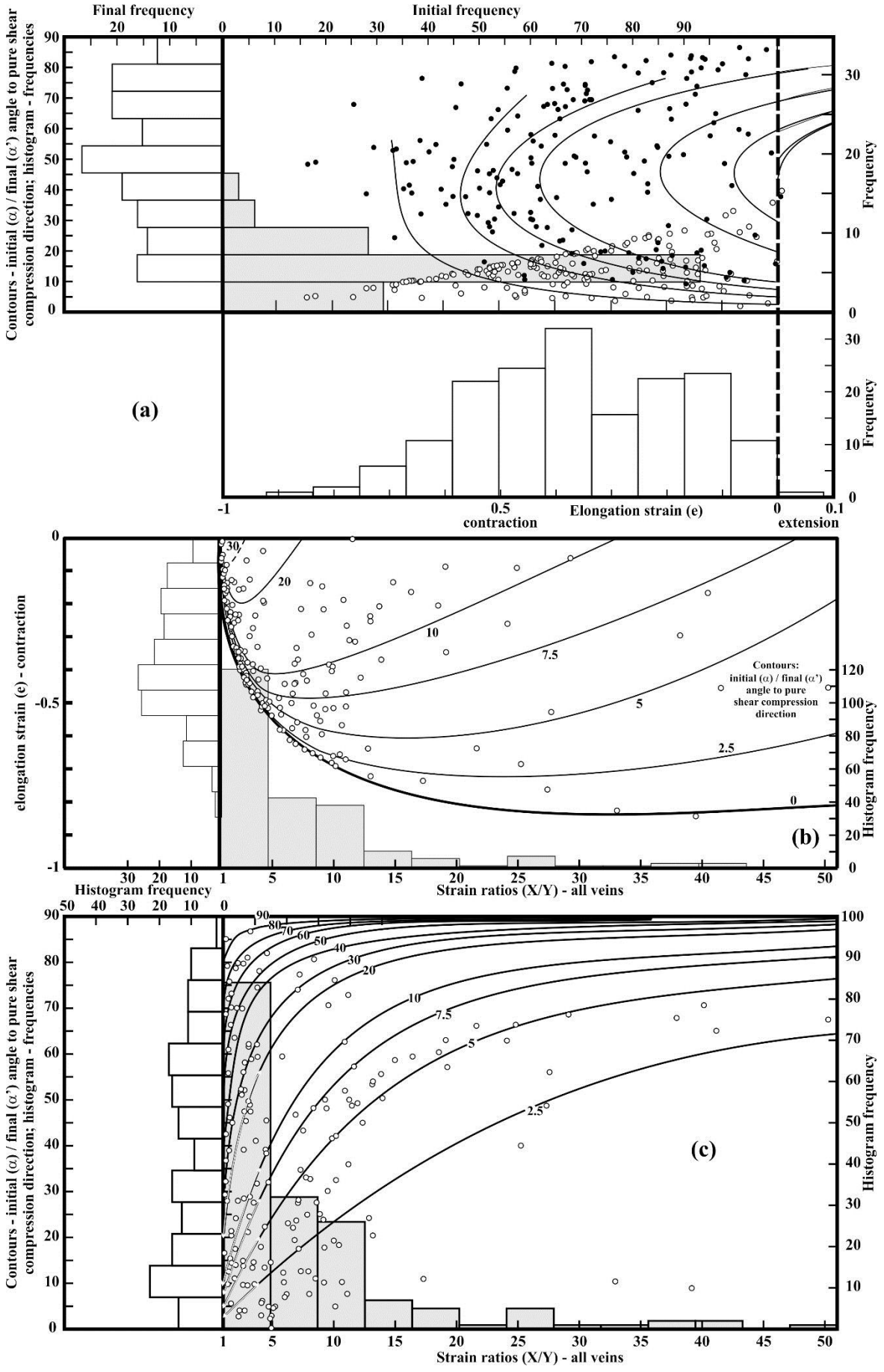
Final frequency
Initial frequency
Contours - initial (α) / final (α') angle to pure shear compression direction; histogram - frequencies
Frequency
(a)
-1
0.5
contraction
Elongation strain (e)
0
0.1
extension
elongation strain (e) - contraction
Contours: initial (α) / final (α') angle to pure shear compression direction
Histogram frequency
(b)
Strain ratios (X/Y) - all veins
(c)

Figure 8

744

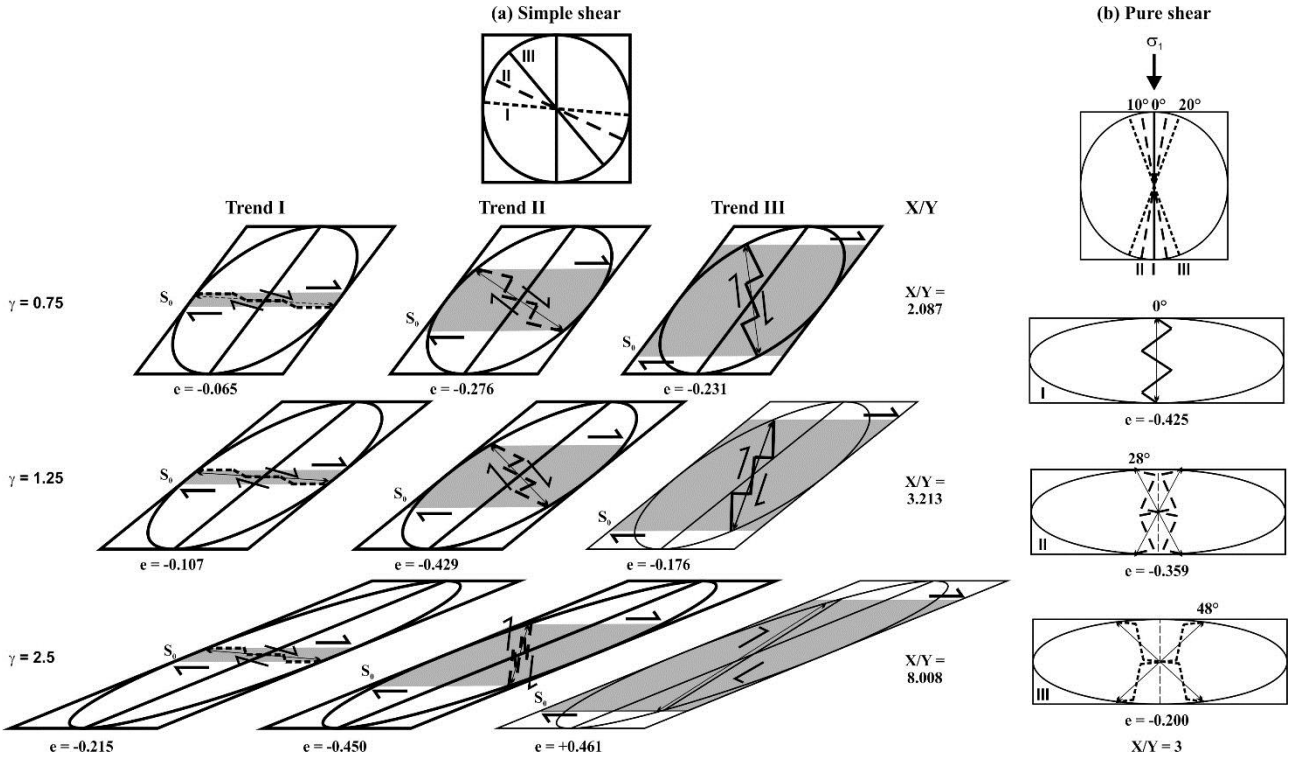
(a) Simple shear
(b) Pure shear
Trend I
Trend II
Trend III
X/Y
γ = 0.75
γ = 1.25
γ = 2.5
e = -0.065
e = -0.276
e = -0.231
e = -0.107
e = -0.429
e = -0.176
e = -0.215
e = -0.450
e = +0.461
X/Y = 2.087
X/Y = 3.213
X/Y = 8.008
10° 0° 20°
0°
28°
48°
e = -0.425
e = -0.359
e = -0.200
X/Y = 3

Figure 9

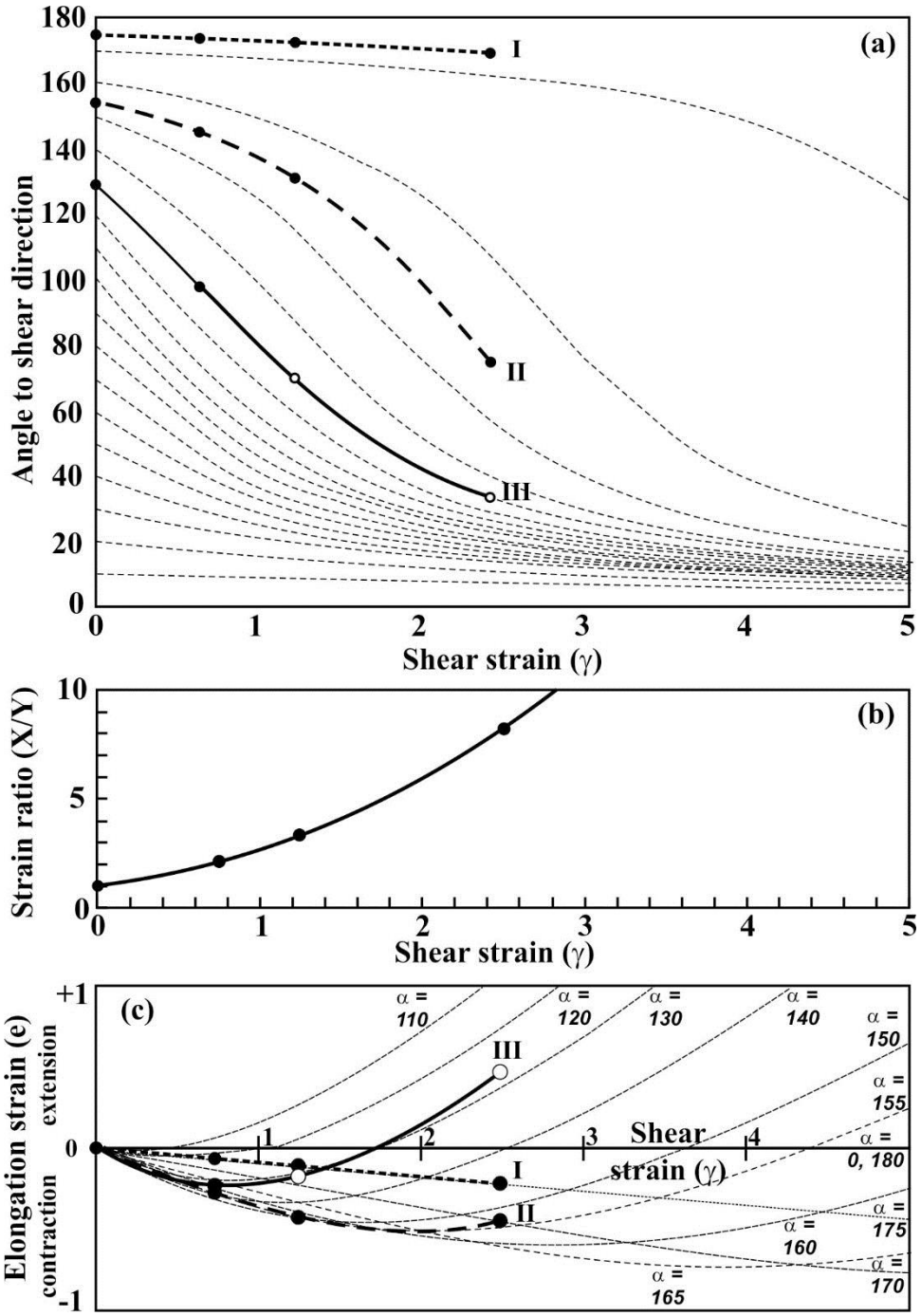

748

749 Figure 10

750

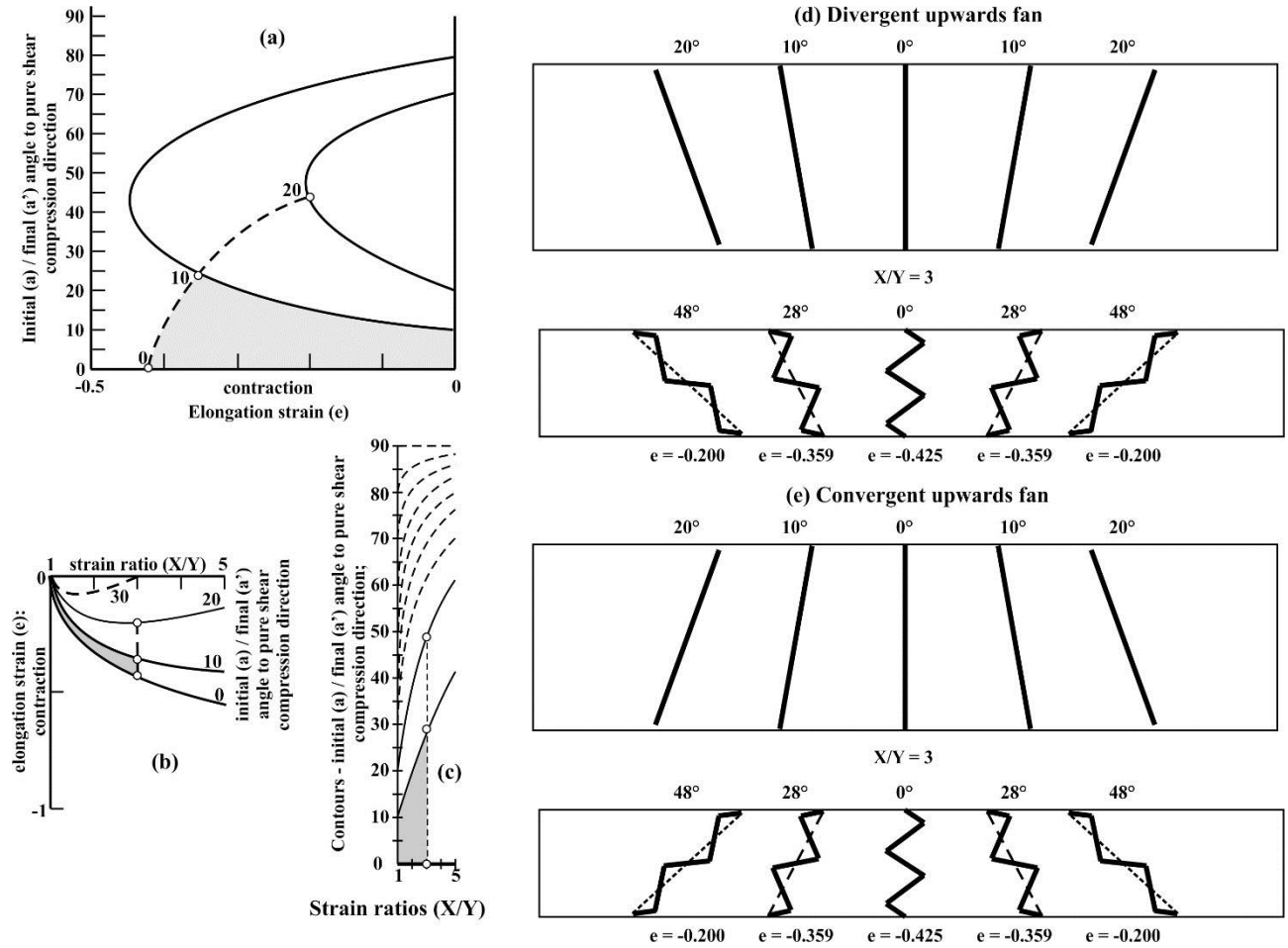
(a)
Initial (a) / final (a') angle to pure shear compression direction
Elongation strain (e)
contraction
(b)
strain ratio (X/Y)
elongation strain (e): contraction
initial (a) / final (a') angle to pure shear compression direction
(c)
Contours - initial (a) / final (a') angle to pure shear compression direction;
Strain ratios (X/Y)
(d) Divergent upwards fan
20° 10° 0° 10° 20°
X/Y = 3
48° 28° 0° 28° 48°
e = -0.200 e = -0.359 e = -0.425 e = -0.359 e = -0.200
(e) Convergent upwards fan
20° 10° 0° 10° 20°
X/Y = 3
48° 28° 0° 28° 48°
e = -0.200 e = -0.359 e = -0.425 e = -0.359 e = -0.200

Figure 11

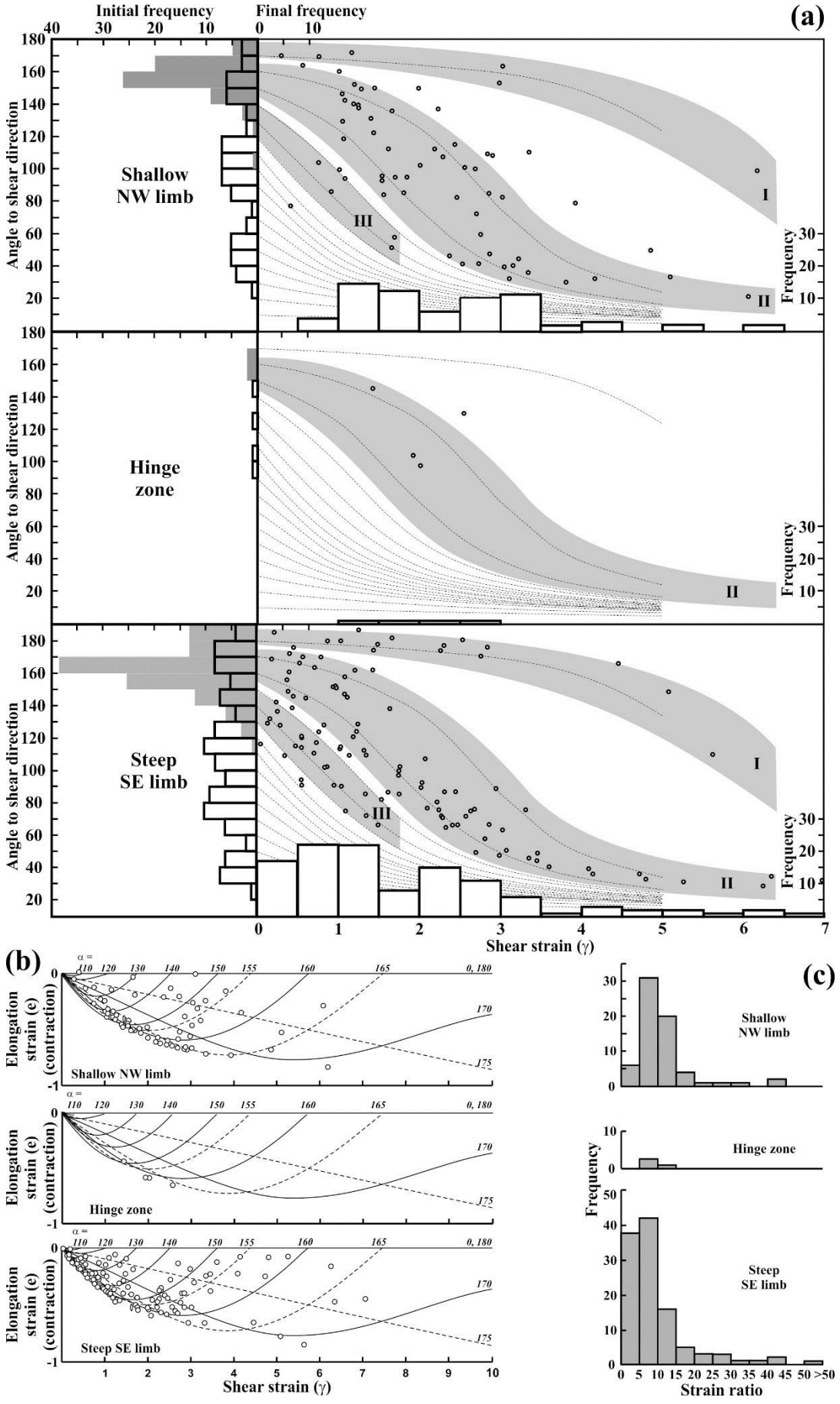
(a)
Initial frequency
Final frequency
Angle to shear direction
Shallow NW limb
Hinge zone
Steep SE limb
I
II
III
Frequency
Shear strain (γ)
(b)
α =
110 120 130 140 150 155 160 165 0, 180
170
175
Elongation strain (e) (contraction)
Shallow NW limb
Hinge zone
Steep SE limb
Shear strain (γ)
(c)
Shallow NW limb
Hinge zone
Steep SE limb
Frequency
Strain ratio

Figure 12

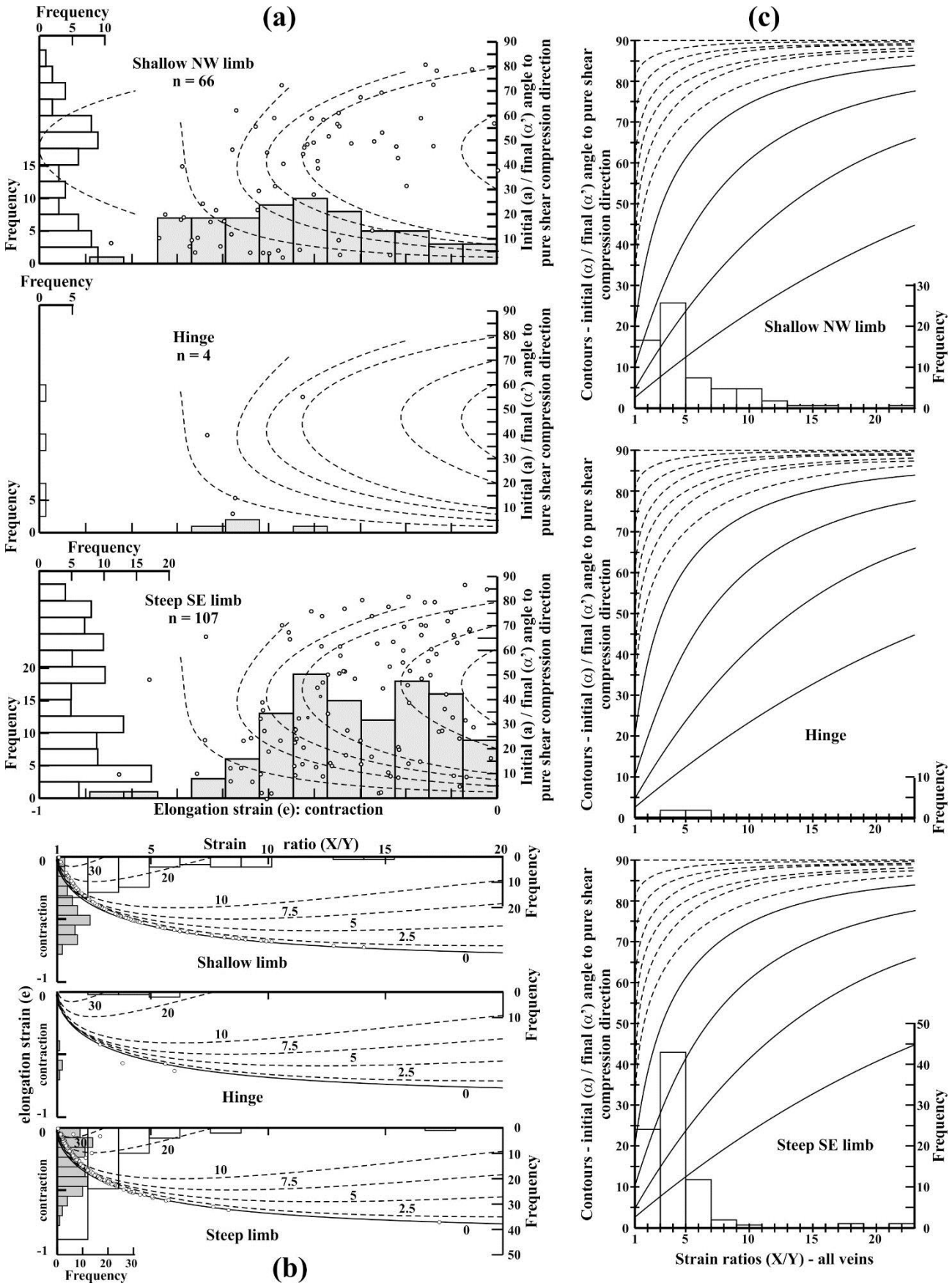
(a)
Shallow NW limb
n = 66
Hinge
n = 4
Steep SE limb
n = 107
Frequency
Initial (a) / final (α') angle to pure shear compression direction
Elongation strain (e): contraction
(b)
Strain ratio (X/Y)
elongation strain (e)
contraction
Shallow limb
Hinge
Steep limb
(c)
Contours - initial (α) / final (α') angle to pure shear compression direction
Shallow NW limb
Hinge
Steep SE limb
Strain ratios (X/Y) - all veins

Figure 13

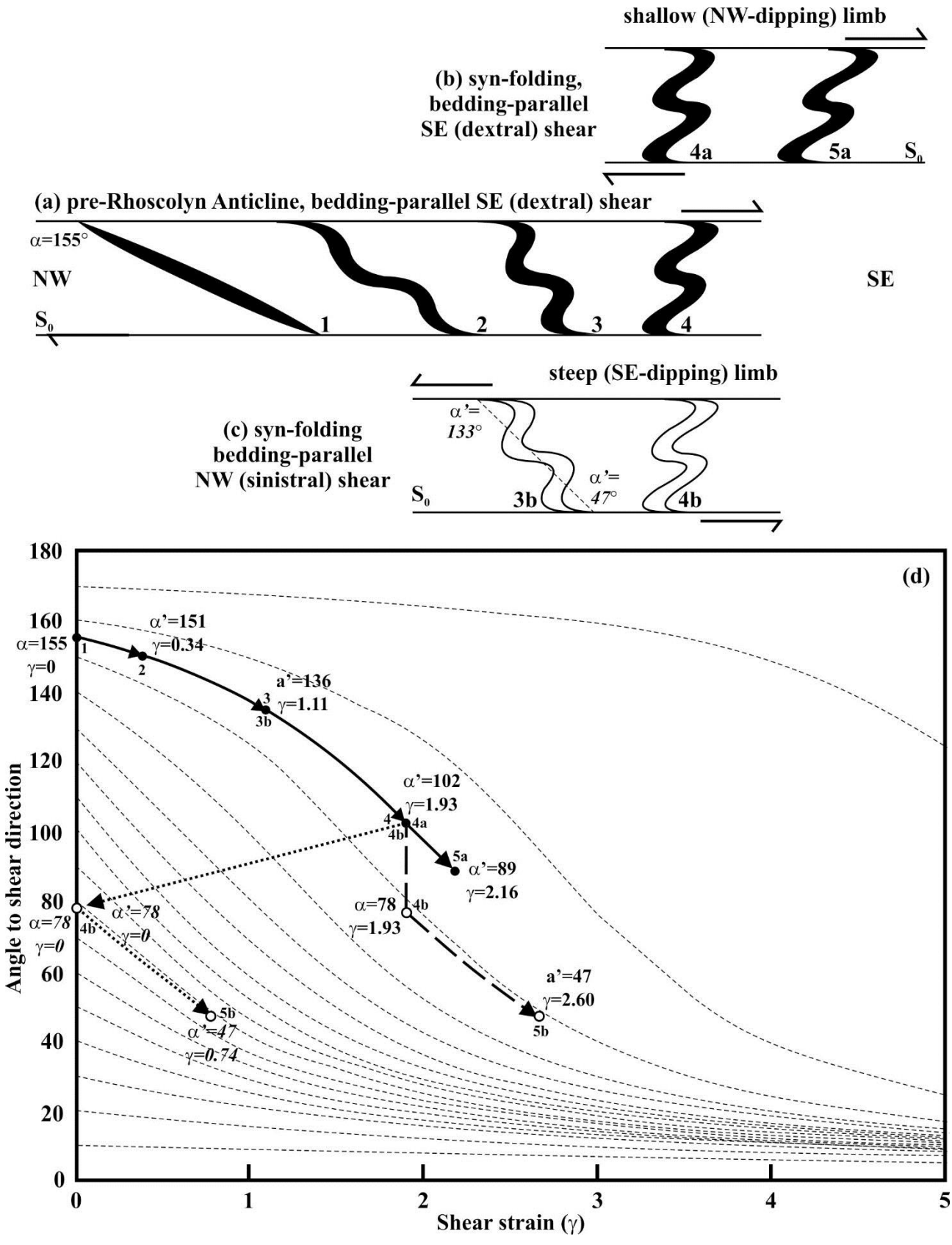
shallow (NW-dipping) limb
(b) syn-folding,
bedding-parallel
SE (dextral) shear
4a
5a
S0
(a) pre-Rhoscolyn Anticline, bedding-parallel SE (dextral) shear
α=155°
NW
S0
1
2
3
4
SE
steep (SE-dipping) limb
(c) syn-folding
bedding-parallel
NW (sinistral) shear
α'=
133°
α'=
47°
S0
3b
4b
(d)
Angle to shear direction
Shear strain (γ)
α=155
γ=0
α'=151
γ=0.34
a'=136
γ=1.11
α'=102
γ=1.93
α'=89
γ=2.16
α=78
γ=1.93
a'=47
γ=2.60
α=78
γ=0
α'=78
γ=0
α'=47
γ=0.74

Figure 14

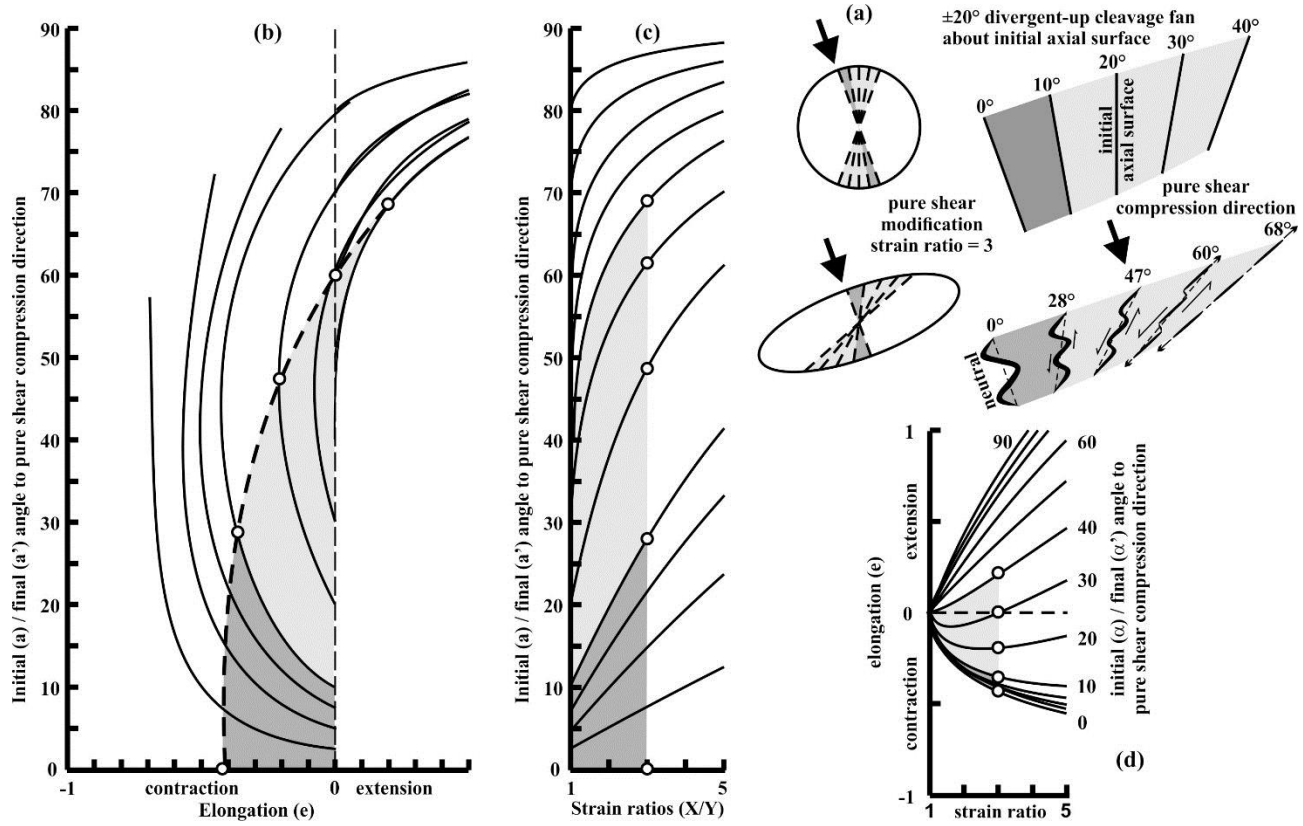

762

763 Figure 15